Nano Research 2015, 8(2): 418–440
DOI 10.1007/s12274-014-0695-5
Review Article
ISSN 1998-0124
CN 11-5974/O4

Enhanced stability of Pt nanoparticle electrocatalysts for fuel cells

Li Li[1,2], Linping Hu[1,2], Jin Li[1], and Zidong Wei[1,2] (✉)

[1] *State Key Laboratory of Power Transmission Equipment & System Security and New Technology, College of Chemistry and Chemical Engineering, Chongqing University, Chongqing 400044, China*
[2] *Chongqing Key Laboratory of Chemical Process for Clean Energy and Resource Utilization, School of Chemistry and Chemical Engineering, Chongqing University, Chongqing 400044, China*

Received: 15 September 2014
Revised: 12 December 2014
Accepted: 14 December 2014

KEYWORDS
Pt catalysts,
stability,
strong metal–support interaction (SMSI),
novel carbon nonmaterial,
hybrid supports

ABSTRACT

Although polymer electrolyte membrane fuel cells (PEMFCs) have received broad attention due to their virtually zero emission, high power density, and high efficiency, at present the limited stability of the electrocatalysts used in PEMFCs is a critical limitation to their large-scale commercialization. As a type of popularly used electrocatalyst material, carbon black supported platinum (Pt/C)—although highly efficient—undergoes corrosion of carbon, Pt dissolution, Ostwald ripening, and aggregation of Pt nanoparticles (NPs) under harsh chemical and electrochemical oxidation conditions, which results in performance degradation of the electrocatalysts. In order to overcome these disadvantages, many groups have tried to improve the carbon support materials on which Pt is loaded. It has been found that some novel carbon nanomaterials and noncarbon materials with high surface areas, sufficient anchoring sites, high electrical conductivities, and high oxidation resistance under the strongly oxidizing condition in PEMFCs are ideal alternative supports. This review highlights the following aspects: (i) Recent advances in using novel carbon nanomaterials and noncarbon support materials to enhance the long-term durability of electrocatalysts; (ii) solutions to improve the electrical conductivity, surface area, and the strong interaction between metal and supports; and (iii) the synergistic effects in hybrid supports which help improve the stability of electrocatalysts.

1 Introduction

Fuel cells (FCs) as a large-scale electrochemical energy conversion system, in combination with the utilization of renewable primary energy resources, are considered to be of crucial importance in tackling the energy crisis and environmental pollution. FCs show promise as a high-efficient energy conversion technology for both mobile and stationary power applications, and have shown great promise for replacing the conventional

Address correspondence to zdwei@cqu.edu.cn

combustion engine for transportation applications [1].

However, the widespread commercialization and deployment of FCs in advanced sustainable energy infrastructures, including the automotive sector, is still limited by two primary factors: (i) High cost and (ii) low lifetime. The high cost is attributed to the insufficient performance, low utilization, and high loading of the expensive platinum (Pt) catalyst materials [2]. For example, the cost of Pt in a hydrogen polymer electrolyte membrane fuel cell (PEMFC) for a 100 kW (134 hp) vehicle is much higher than that for an entire 100 kW gasoline engine. According to the cost reduction targets set by the U.S. Department of Energy (DOE) [3], the total Pt catalyst loading (on both anode and cathode) in a membrane electrode assembly (MEA) must be reduced to below 0.125 $mg \cdot cm^{-2}$. To lower the catalyst cost, highly dispersed ultra-small metallic Pt and its alloy nanoparticles (NPs, 2–5 nm) have been made with a uniform distribution on high surface area carbon black supports [4]. However, smaller particles have shown worse durability, and attempts to decrease cost by increasing the dispersion and decreasing the particle size always decrease durability [5]. A FC typically operates under almost steady-state conditions below 1.0 V, while during start-up and shut-down (start–stop) cycles, the electrode potential can locally reach values up to 1.5 V. At such a high potential, the degradation in both performance and durability of the Pt/C catalyst is significantly accelerated. Besides the high voltage, the acidic and oxidizing environment in PEMFCs resulting from the presence of H_2O_2, O, and OH species, and the impurities in the air including SO_x, NO_x, and H_2S also have a strong influence on the durability of Pt/C catalyst. Therefore, the long-term stability of Pt and Pt-alloy electrocatalysts as requested by the U.S. DOE FC targets ($30 per kW and a lifespan of 5,000 h) [3], especially under the conditions the oxygen reduction reaction (ORR) involves, still remains a challenge.

In PEMFCs operation, Pt NPs will also suffer from poor durability because of the rapid and significant loss of the Pt electrochemical surface area (ECSA) over time. The well-known reasons include corrosion of the carbon support, Pt dissolution, Ostwald ripening, and aggregation. The corrosion of carbon support and Pt dissolution are believed to be the major primary degradation mechanisms [6]. Thus, increasing the stability of the support, enhancing the oxidation resistance of Pt NPs, and increasing the interaction between the Pt NPs and supports are all critical strategies to improve the durability of a FC. The most widely used approaches in this respect are: (i) Substituting the carbon black support with novel highly graphitized carbon nanomaterials such as carbon nanotubes (CNTs) [7, 8] and graphene [9–11], or with noncarbon catalyst supports, including transition metal oxides [12–14] and nitrides [15, 16]; and (ii) designing Pt-based alloy NPs with various nanostructures such as core/shell [4] and nanoframes [17].

To evaluate long-term durability of PEMFC systems and their components, several types of accelerated stress tests (AST) have been developed including [18, 19] (i) thermal degradation under hot air conditions, (ii) reduced humidity, (iii) open circuit cell operation, and (iv) electrochemical forced aging under simulated cell conditions. Compared with other degradation testing protocols, electrochemical forced aging, i.e., a three-electrode half-cell system employed in an aqueous acid solution (H_2SO_4 or $HClO_4$), has been applied widely [20]. Electrochemical forced aging generally includes potential cycling tests and potential holding tests. Up to now, several different potential cycling windows, for instance, 0–1.2 V [21], 0.6–1.0 V [22], 0.6–1.1 V [23], and 0–1.4 V [24], have been employed to evaluate the catalyst durability.

The aim of this review is to summarize the current developments in enhancing the stability of supported Pt NP electrocatalysts for FCs. Recently Su et al. [5] reviewed the improvements in durability of Pt-based cathode catalysts afforded by incorporating another noble metal or adjusting the material nanostructure and morphology. Thus, the present review mainly focuses on the effect of the interactions between the support and Pt NPs on the durability of the Pt/C catalyst. It covers: (1) The degradation mechanism of Pt/C catalysts; (2) the stability of the Pt NPs supported on carbon materials including carbon black, CNTs, graphene, and other novel carbon nanomaterials; (3) the stability of the Pt NPs supported on noncarbon catalyst supports including the metal oxides, metal carbides, metal nitride, and other hybrid supports; (4) an outlook on the future trends and developments in this area.

2 Degradation mechanism of Pt/C catalysts

The durability of a catalyst support is currently a technical barrier for the commercialization of PEMFCs. At present, almost all PEMFCs employ carbon-supported catalysts, especially Vulcan XC72 carbon black because of its large surface area, high electrical conductivity, and well-developed pore structure. Pt/C is widely used as an electrocatalyst in FCs because of its relatively high activity for the ORR. However, loss in active Pt surface area occurs during FC operation as a consequence of the degradation of both catalyst and support. Regarding Pt/C catalysts, major research efforts over the last decades have been made to explore the degradation mechanism and improve the durability of the Pt/C catalysts. Several mechanisms have been proposed for the degradation of Pt/C catalysts [5, 25, 26]. First is the corrosion of the carbon support, which directly initiates the detachment and aggregation of Pt NPs. Second is the dissolution of Pt from smaller particles. Third is the growth of Pt NPs via Ostwald ripening and aggregation. This includes the redeposition of the soluble Pt species onto larger particles and the coalescence of Pt NPs via migration on the carbon support surface. The last mechanism involves detachment of complete particles from the support. The degradation process of Pt/C catalysts is illustrated in Fig. 1 [27]. In these proposed mechanisms, the corrosion of the carbon support and Pt dissolution are considered as the primary degradation mechanisms.

The corrosion of the carbon support is the major primary degradation mechanism [6, 25, 28, 29]. The corrosion of carbon in acidic electrolytes involves the reaction [30]

$$C + H_2O \rightarrow CO_2 + 4H^+ + 4e^-, E_0 = 0.207 \text{ V vs. RHE} \quad (1)$$

This reaction is thermodynamically feasible at the potentials at which the cathode operates (typically 0.6–1.0 V vs. the reversible hydrogen electrode (RHE)) but occurs at very low rates in this potential range as a result of the inherently slow kinetics. But during FC startup and shutdown in automotive applications, the operation potential can be up to 1.5 V [29, 31]. At these high potentials, the carbon corrosion reaction is significantly accelerated, leading to irreversible carbon loss at the electrode. Inevitably, the carbon corrosion at the Pt/C interface initiates a series of secondary degradation processes. For example, electrochemical corrosion of carbon causes electrical isolation of the catalyst particles as they are separated from the support and also leads to aggregation of catalyst particles. Meier et al. [29] proved that the detachment of Pt NPs from the carbon support and the agglomeration of Pt NPs are a direct consequence of the severe oxidation of the carbon support and the concomitant structural and chemical changes. Simultaneously, oxidation of the carbon surface also induces an increase in surface hydrophilicity, which leads to condensed phase mass transport limitations resulting from water retention within the pores of the catalyst. Furthermore, the

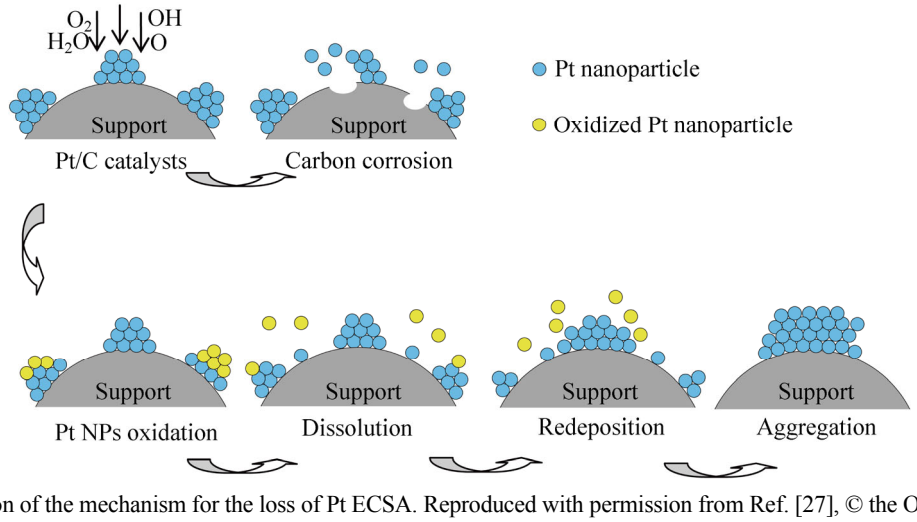

Figure 1 Illustration of the mechanism for the loss of Pt ECSA. Reproduced with permission from Ref. [27], © the Owner Societies 2012.

presence of Pt can accelerate the corrosion rate of the carbon support. Thus, it is very crucial to improve the stability of the support.

In addition to corrosion of carbon, Pt dissolution is another major primary degradation mechanism [32–35]. The potential dependence of Pt dissolution is invoked as the source of the observed potential dependence of ECSA loss rate, particle growth, and Pt loss into the membrane. Although Pt is thermodynamically stable towards dissolution in a large pH and potential window, according to its Pourbaix diagram, Pt is susceptible to dissolution at potentials higher than 0.85 V vs. RHE at pH values lower than 2 (at 25 °C), where PEM cathode FC catalysts are employed [36]. The Pt dissolution takes place through either a direct pathway or an indirect pathway involving the formation of Pt oxide (Eq. (2)) and the chemical dissolution of oxide (Eqs. (3) and (4)) [37, 38]

$$Pt \rightarrow Pt^{2+} + 2e^{-}, E_0 = 1.188\ V \quad (2)$$

$$Pt + H_2O \rightarrow PtO + 2H^{+} + 2e^{-}, E_0 = 0.980\ V \quad (3)$$

$$PtO + 2H^{+} \rightarrow Pt^{2+} + H_2O + 2e^{-} \quad (4)$$

The Pt dissolution was demonstrated to be dependent on the particle sizes and oxide coverage [35, 39]. The dissolution rate increases with decreasing particle size, and particles with diameters smaller than 2 nm are expected to dissolve orders of magnitude faster than particles with diameters of, for instance, 5 nm, owing to the Gibbs–Thomson effect [33]. In addition, particles with smaller sizes can be dissolved by direct electro-oxidation of metallic Pt to give soluble Pt^{2+} cations, unlike bulk Pt, which is dissolved via its oxides [31, 40]. The strong influence of Pt dissolution on the overall degradation behavior emphasizes the importance of enhancing the oxidation resistance of Pt particles.

A third proposed mechanism of ECSA loss is particle growth via Ostwald ripening and agglomeration [37, 38, 41, 42]. Ostwald ripening is a secondary degradation mechanism strongly linked to the primary process of Pt dissolution [41, 42]. It involves inter-particle transport of mobile species, with larger particles growing at the expense of smaller particles. In other words, small particles dissolve into the electrolyte and shrink, while the dissolved Pt is redeposited on larger platinum particles driven by difference in surface free energy and local adatom concentration on the support surface. Agglomeration (particle migration and coalescence) is a second possible explanation for the observed particle growth in FCs [41]. It involves the Brownian motion of NPs leading to coalescence when particles come in close proximity to each other. Migration of Pt particles and successive agglomeration has been suggested to be responsible for coarsening. Moreover, the corrosion of the support can also induce Pt particle agglomeration, as Pt particles in proximity to each other come into contact when the support shrinks.

The last mechanism involves detachment of complete particles from the support [37, 38]. In general, the detachment results from a weakening of the interaction between the platinum particles and the carbon support, for instance, by direct corrosion of carbon at the interface. It should be noted that agglomeration and detachment are observed in parallel because both processes imply a weakening of the interaction between Pt particles and carbon supports.

3 Stability of Pt NPs supported on different carbon supports

3.1 Carbon black

Conductive carbon black (CB) is currently widely used as a support for catalyst nanoparticles because of its easy availability and low cost [28]. The commonly used carbon black support materials, together with some properties are listed in Table 1 [43]. Among these carbon blacks, Vulcan XC72 carbon is the most widely used owing to its more abundant defect sites and organic-surface groups, which lead to a more homogenous Pt dispersion. For example, Speder et al. [44] used a colloidal synthesis approach to support Pt nanoparticles on two commercial carbon blacks, namely Vulcan XC72R and Ketjenblack EC300J. They found that the Pt/Vulcan shows a higher ECSA value than that of the Pt/EC300J, although the Brunauer–Emmett–Teller (BET) surface area of EC300J is considerably higher than that of Vulcan. This is because that the Vulcan support possesses a larger number of defect sites, which enables a better and more homogenous Pt

Table 1 Carbon blacks that have been used as support for Pt catalysts in PEMFCs [43]

Carbon	Supplier	Type of carbon	BET surface area ($m^2 \cdot g^{-1}$)	DBP adsorption (unit)[a]
Vulcan XC72	Cabot Crop.	Furnace black	250	190
Black Pearls 2000	Cabot Crop.	Furnace black	1,500	330
Ketjen EC300J	Ketjen Black International	Furnace black	800	360
Ketjen EC600JD	Ketjen Black International	Furnace black	1,270	495
Shawinigan	Chevron	Acetylene black	80	—
Denka black	Denka	Acetylene black	65	165

[a] DBP: dibutyl phthalate number (measure of carbon void volume).

dispersion, while the porous structures of Ketjenblack may lead to the encapsulation of some Pt NPs inside the pores so that they become inaccessible.

However, the large number of defect sites, by enhancing the thermochemical instability of CB under the operation condition of FCs, also causes the degradation of catalysts. Speder et al. [44] also found that Vulcan samples exhibit higher ECSA losses than those of the Ketjenblack samples due to the carbon corrosion under start–stop conditions (cycling between 1.0 and 1.5 V vs. RHE with a sweep rate of 500 $mV \cdot s^{-1}$). After 15 h AST treatment, an ECSA loss of 35% was observed for the 30 wt.% Pt/Vulcan catalyst, compared to an 18% loss for the 30 wt.% Pt/Kejenblack. The higher carbon corrosion on Vulcan is due to its larger number of defect sites. Additionally, Wang et al. [45] compared the durability of Pt NPs supported on XC72 and Black Pearls 2000 (BP-2000). Their electrochemical measurements indicated a higher ECSA degradation rate (40.9%) for Pt/BP-2000 after AST (potential cycling in the window 0.6–1.2 V) than the value of 20.6% for Pt/XC72. The higher degradation rate of the Pt/BP-2000 catalyst results mainly from the lower corrosion resistance of BP-2000, which further induces the dissolution and growth of Pt NPs.

An effective method to avoid the corrosion of carbon supports is to add a protector to prevent the carbon supports from direct exposure to the corrosive environment. Chen et al. [21] designed and synthesized a polyaniline (PANI)-decorated Pt/C@PANI core–shell catalyst through direct polymerization of a thin layer of PANI on the carbon surface of a Pt/C catalyst (Figs. 2(a)–2(d)). The PANI shell affords good environmental stability, high electrical and proton conductivity, and unique redox properties, and thus acts as a good protector for Pt/C@PANI catalyst by playing three important roles. One is to avoid directly contact between the carbon support and the corrosive environment. The second is to strengthen the interactions between Pt NPs and the support, thus successfully inhibiting agglomeration of Pt NPs. The third is to improve the catalytic activity of Pt/C by changing the electronic configuration of Pt. The as-made Pt/C@PANI catalysts exhibited high catalytic activity, excellent stability, and long-term durability, even after AST (Figs. 2(e) and 2(f)). Density functional theory (DFT) calculations [46] showed that the number of holes in PANI increased with the continuous electron transfer from PANI to the carbon support, which caused partial oxidation of PANI and thus increased its electric conductivity. PANI interacted with Pt/C mainly via three C atoms or one N atom and two C atoms within the same benzene ring. The system energy decreased markedly with increasing coverage of PANI on the Pt/C, which meant that the Pt/C@PANI was more stable than Pt/C. The raised highest occupied molecular orbital (HOMO) energy level and lowered d band center of Pt/C@PANI compared with Pt/C favor the electron transfer between Pt/C@PANI and O_2 due to the reduced gap between the Pt/C@PANI HOMO and the oxygen lowest unoccupied molecular orbital (LUMO), which also facilitated the desorption of intermediate species on the surface of the catalyst and increased the generation of fresh catalytic sites for the subsequent reaction (Figs. 2(g) and 2(h)).

3.2 Carbon nanotubes

CNTs have emerged as a promising support material for FC catalysts due to their large surface area, high electrical conductivity, and excellent electrochemical

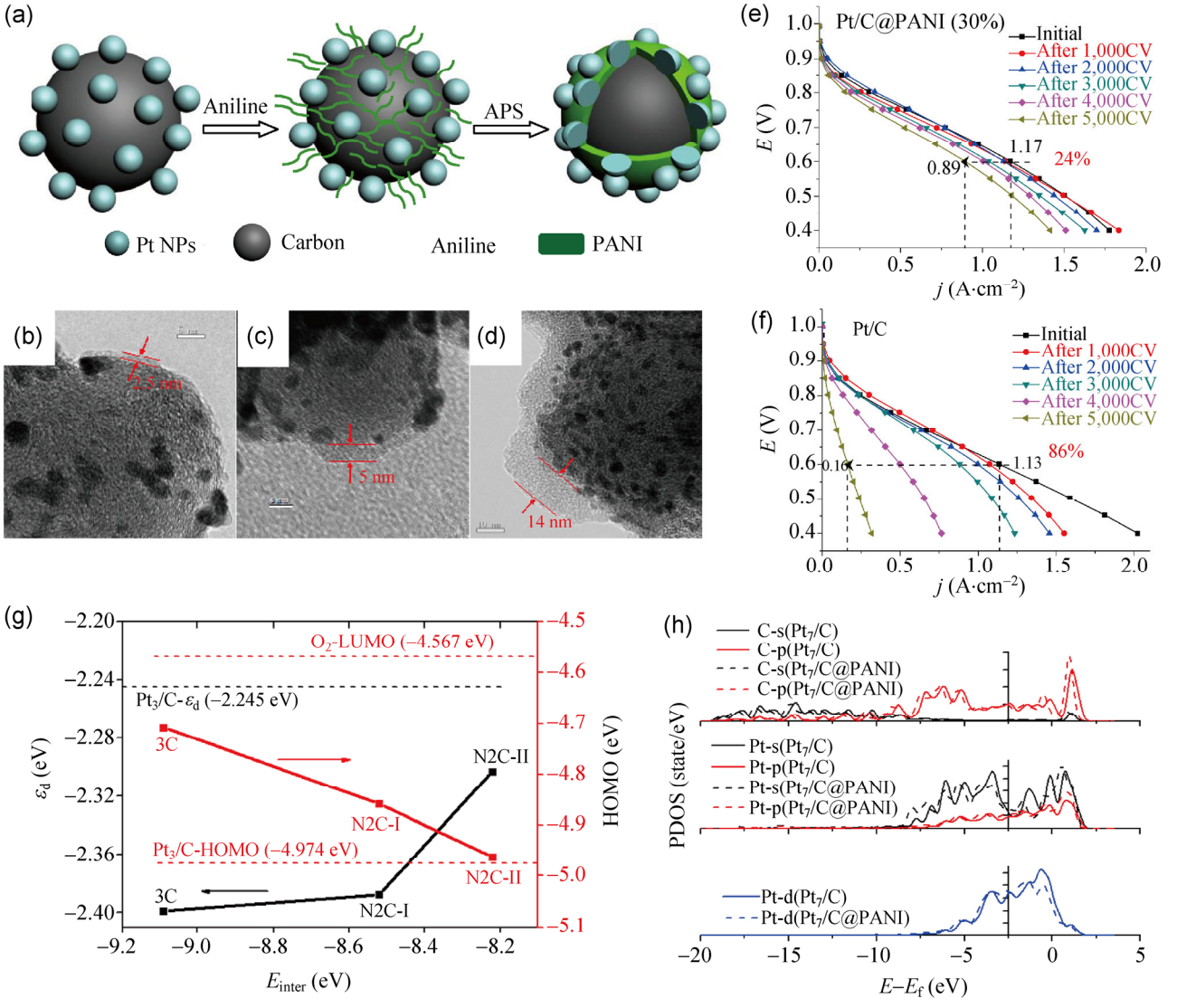

Figure 2 (a) Configuration of the Pt/C@PANI catalyst. HRTEM images of the Pt/C@PANI catalysts with PANI loadings of (b) 20%, (c) 30%, and (d) 50%. Polarization curves of single PEM fuel cell with cathodes fabricated from (e) PANI@Pt/C (30%) and (f) Pt/C catalysts after the indicated numbers of CV cycles, the Pt loading was 0.3 mg·cm^{-2} on the anode and 0.2 mg·cm^{-2} on the cathode. (g) d-band center and the HOMO energy level of Pt_3/C@PANI (3C, N_2C-I, N_2C-II). (h) Density of states of C and Pt atoms of the Pt_7/C and Pt_7/C@PANI. Reproduced with permission from Ref. [21], © American Chemical Society 2012, and Ref. [46], © Science China Press 2013.

durability. However, pristine CNTs contain relatively few binding sites for anchoring the Pt precursors or Pt NPs due to the high curvature and chemical inertness of the CNT surface. As a result, Pt/CNT catalysts generally have poor Pt dispersion and large Pt NPs, especially when the Pt loading is high. Thus, how to evenly deposit Pt NPs on the surfaces of CNTs and reinforce the binding strength between the two phases are major challenges.

In general, the best established protocols for catalytic metal immobilization on CNTs include introducing defects and oxygen-containing functional groups, such as carboxyl and hydroxyl groups, on the external walls by harsh acid oxidization, such as refluxing in HNO_3 followed by metal deposition on activated CNTs walls. However, the presence of defect sites and the oxygen-containing functional groups largely destroy the graphitized CNTs surface, and thus reduce the conductivity and accelerate the corrosion of CNTs. These drawbacks lead to low output performance for

Pt/CNT catalysts in PEMFCs.

In order to overcome the above barriers, many studies have focused on the surface treatment of CNTs. The methods employed involve (i) using special organic functional groups, functional polymers, and heteroatoms including N, P, S, and F atoms [47] to modify CNT surfaces, and (ii) using homogeneous silica [7, 48] or metal oxides [49–52] (such as TiO_2 or SnO_2) shell to link metal NPs and CNTs. Evidence shows that such treatments are effective since they do not break the continuity of CNTs, and enhance the nucleation of Pt NPs onto the inert surfaces of the CNTs.

Wei's team [27, 53] found that an ideal organic functional group on the CNTs used for stabilization of supported Pt NPs should not only provide a deposition and anchoring site for Pt NPs, but also maintain the original perfect structure of CNTs rather than destroying it. So far some functional groups, such as thiol groups [53–55], amine groups, and aniline [56] have been found to be able to enhance the stabilization of the Pt NPs. For instance, Chen et al. [53] reported a novel thiolated CNT (SH-CNT) support by directly linking thiol groups on the CNT surface (Fig. 3(a)). DFT calculations [27] indicated that –SH groups on the CNT surface enhance the oxidation resistance of the Pt clusters and CNTs, and restrict Pt migration on the CNTs. Experiments verified that the thiolated CNTs have abundant –SH groups on their surface, which serve as anchoring centers for achieving high Pt dispersion and ensure the high activity of the catalysts. Moreover, the –SH groups can enhance the interaction between the Pt NPs and CNTs, which is very helpful to inhibit the dissolution, Ostwald ripening, and coalescence of Pt NPs. AST shows that the Pt ECSA of Pt/SH-CNTs catalyst only decreased approximately by 22.3% after 1,500 CV cycles, whereas the Pt/pristine-CNTs and Pt/COOH-CNTs catalysts

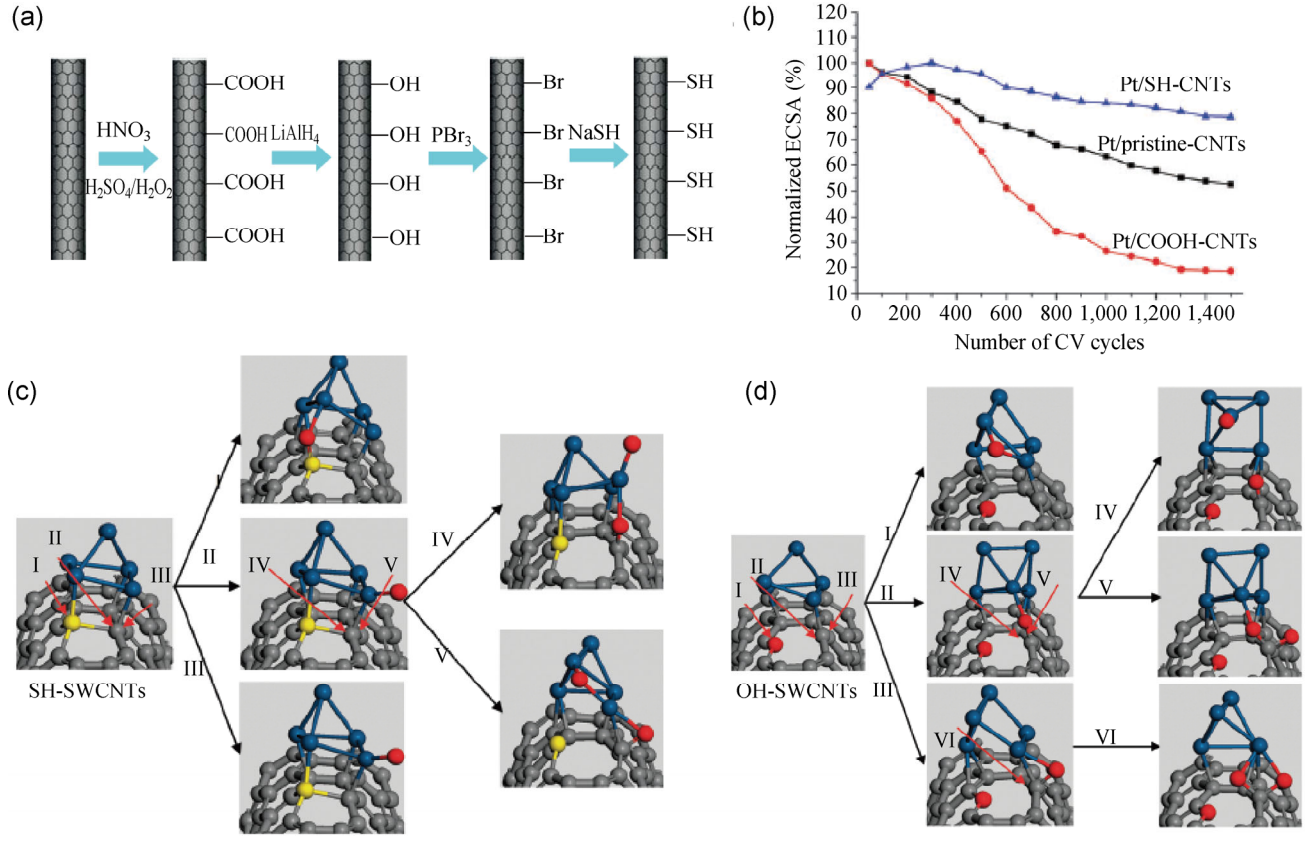

Figure 3 (a) Schematic illustration of the synthetic procedure for SH-CNTs. (b) Normalized Pt ECSA of electrodes made with Pt/SH-CNTs, Pt/pristine-CNTs, and Pt/COOH-CNTs catalysts in N_2-purged 0.5 M H_2SO_4 at room temperature (0–1.2 V vs. RHE, sweep rate 50 mV·s^{-1}). Attack configurations of O_{ad} on (c) Pt_5/SH-SWCNTs and (d) Pt_5/OH-SWCNTs. Reproduced with permission from Ref. [27], © the Owner Societies 2012, and Ref. [53], © the Royal Society of Chemistry 2011.

lost about 48.1% and 81.3% of their initial ECSA, respectively (Fig. 3(b)). The strong interactions between thiolated CNTs and Pt NPs also have been verified by Park et al. [55]. They investigated the effect of the electronic interaction between Pt NPs and various functional groups on carbon supports, such as thiols, amines, carboxylate, and carbon basal planes, on the Pt dissolution. A strong interaction was found only in Pt/SH-CNTs. The theoretical basis for the markedly enhanced tolerance of Pt/SH-CNTs against Pt dissolution was ascribed to the charge compensation from S to Pt at high potentials. Thus, the functional groups on the CNTs used for stabilization of supported Pt NPs should provide a deposition and anchoring site to enhance the Pt–CNTs interaction, and maintain the perfect structure of the CNTs rather than destroying it.

Besides functional groups, conducting polymers as a linker between metal NPs and CNTs can also improve the stability of Pt/CNTs. To date, several polymers including polyallylamine hydrochloride, polypyrrole (PPy), polydiallyldimethylammonium chloride (PDDA) [57], polyaniline (PANI) [58], imidazolium-salt-based ionic liquids (Is-ILs) [59], and polybenzimidazole (PBI) [60] have been used to anchor metal NPs onto the surface of CNTs. The advantages of polymer wrapping of CNTs include: (i) Non-destructive modification leading to good preservation of the electrochemical durability, and (ii) stabilization of the uniform CNT surface modification via effective loading of metal NPs. Fujigaya et al. [60] reported an "*in situ* surface growth method" to fabricate Pt-loaded CNTs using PBIs as linker polymers, by means of which binding sites could be non-covalently introduced onto a CNT surface. PBI, recognized as a powerful candidate for use in FCs due to its high proton conductivity at a temperature of above 100 °C under non-humid conditions, has a strong physical interaction with CNTs and serves as an effective binding site for loading of Pt NPs. A schematic of the structure of Pt/PBIs/CNTs is shown in Fig. 4(a). Due to the non-destructive functionalization of the CNTs, the Pt/PBIs/CNTs showed higher electrocatalytic activity and better stability for the ORR than Pt NPs supported on chemically-modified-CNTs and CB. In addition, the Pt/PBIs/CNTs have a larger ECSA than that of Pt/CNTs. Such large ECSA values clearly indicate that the

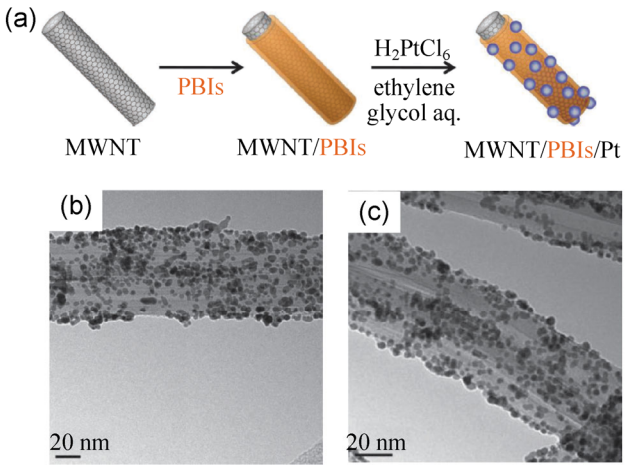

Figure 4 (a) Schematic drawing of the preparation of MWNT/PBIs/Pt, and TEM images of (b) MWNT/PhPBI/Pt and (c) MWNT/PyPBI/Pt. Reproduced with permission from Ref. [60], © WILEY-VCH Verlag GmbH & Co. KGaA, Weinheim 2013.

dispersed Pt NPs are well exposed to the electrolyte solution, as shown in Figs. 4(b) and 4(c). The interface structure of Pt/PBIs/CNTs is most likely the "ideal" triple-phase boundary structure that enables excellent FC catalyst efficiency.

3.3 Graphene

Graphene has recently emerged as a highly promising catalyst support material for PEMFC applications owing to its high conductivity (10^3–10^4 S·m^{-1}), fast charge-transport mobility, good transparency, great mechanical flexibility, astonishing elastic properties, and huge specific surface area (theoretically 2,630 m^2·g^{-1} for a single layer) [9, 61]. Graphene is as a one-atom-thick planar sheet of hexagonally arrayed, two-dimensional (2D) sp^2 carbon atoms, which can provide added resilience against carbon corrosion during PEMFC operation. However, the relatively inert and hydrophobic nature of the graphene surface does not facilitate the deposition of Pt NPs. To obtain well-dispersed nanoparticles and overcome stability limitations, graphene can be functionalized with heteroatoms [62] such as N, P, B, S, and Se, among which N has larger electronegativity than carbon, P and B have lower electronegativity than carbon, and S and Se have the similar electronegativity to carbon. In addition, binary and ternary doped graphene materials have also been developed recently as catalyst supports in

order to strengthen further Pt adsorption on graphene [11, 63, 64].

N-doped graphene (NG) [65] has been considered as an ideal support for metal NPs to form catalysts, because N-doping can introduce chemically active sites for reaction and anchoring sites for metal NPs deposition, modify electronic properties and give carbon materials a n-type or metallic behavior. There are three types of N atoms, which are pyridinic, pyrrolic, and quaternary N. Of these, only the pyridinic and pyrrolic forms have planar structures with high conductivity. In contrast, quaternary N atoms with a three-dimensional (3D) structure have relatively low electrical conductivity, resulting from the interruption of their π–π conjugation by the 3D structure [66]. In addition, the extent of dispersion of Pt NPs increases with increasing N content, and the pyridinic-N sites can enhance the adhesion between Pt NPs and supports, and stabilize Pt in a more dispersed state [67–70].

For example, Vinayan et al. [71] developed a novel method for uniform coating of conductive polymers, such as polypyrrole, over a graphene surface using an anionic polyelectrolyte. N-doping of graphene was achieved by pyrolysis of the PPy-modified graphene nanocomposite. The amount of N incorporated in graphene was about 5.9 at.%, and the pyridinic-N atom was the main component of the N-doped graphene (NG). These NG sheets were used as a catalyst support for dispersing Pt and Pt–Co alloy NPs synthesized by the modified-polyol reduction method, yielding a uniform dispersion of the catalyst NPs, as shown in Figs. 5(a), 5(c), and 5(d). Compared with commercial E-TEK Pt/C electrocatalysts, Pt/NG and Pt_3Co/NG showed excellent performances, being, respectively, 2.41 and 4 times higher than that of a commercial Pt/C catalyst. The superior performance of the Pt_3Co/NG

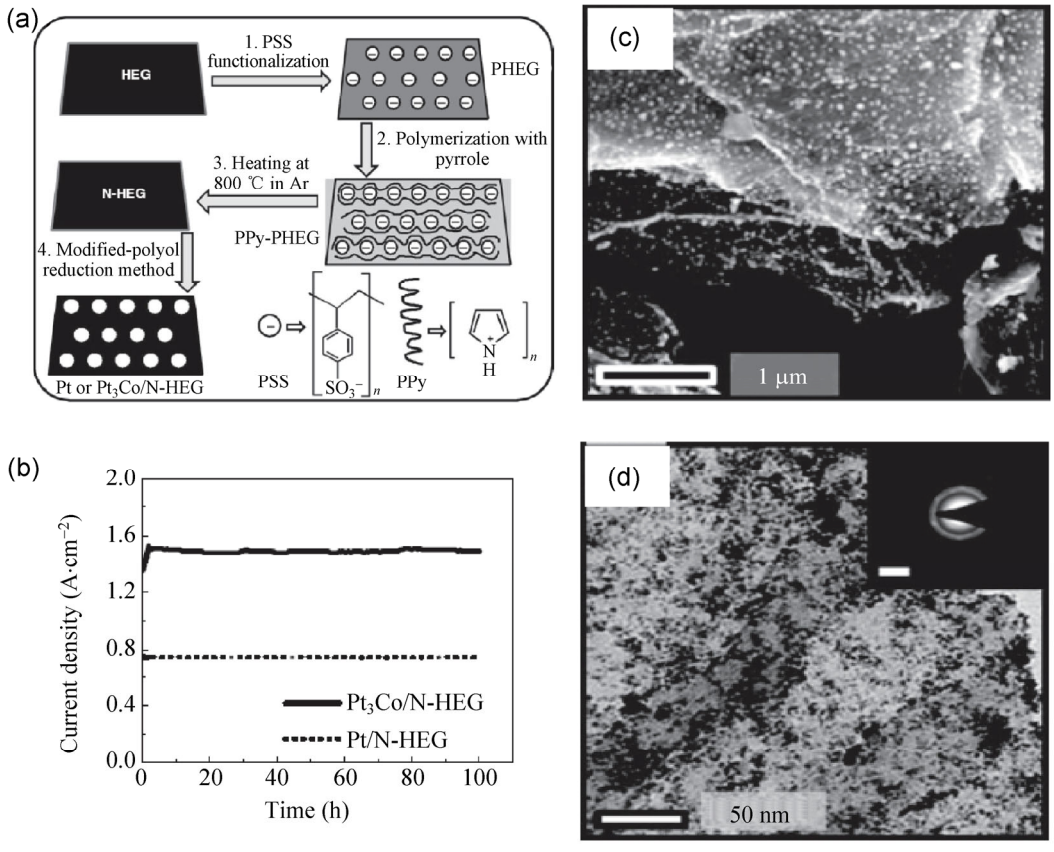

Figure 5 (a) Schematic illustration of the synthesis procedure of Pt/N-HEG. (b) Stability study of the PEMFC with cathode electrocatalyst containing Pt/N-HEG and Pt_3Co/N-HEG at 60 ˚C without any back pressure. (c) SEM and (d) TEM images of Pt/N-HEG. The inset in (d) shows the electron diffraction pattern of Pt/N-HEG. The scale bar is corresponding to 5 nm^{-1}. Reproduced with permission from Ref. [71], © WILEY-VCH Verlag GmbH & Co. KGaA, Weinheim 2012.

is attributed to the combined effects of the modified Pt state due to alloying and N-doping, along with a uniform dispersion of catalyst NPs. The stability of Pt/NG and Pt_3Co/NG cathode catalysts was studied by running a membrane electrode assembly (MEA) assembled with a Pt/C anode catalyst for 100 h at a voltage of 0.5 V at 60 ℃ without any back pressure. The MEAs with Pt/NG and Pt_3Co/NG as cathode catalyst displayed no performance degradation at 0.5 V for 100 h, showing the high stability of the electrocatalyst (Fig. 5(b)). Doping of N atoms results in strong binding between metal NPs and the graphene surface, which prevents the detachment of metal NPs from the graphene support and their agglomeration during cell operation, thereby increasing the long-term stability of the electrode. Similarly, He et al. [69] also showed that an NG with pyridinic-N as the dominant N species can improve the activity and stability of Pt/NG catalysts effectively. Thus, the synthesis of NG materials with higher amount of N in graphene and with more planar pyridinic and pyrrolic N atoms and fewer quaternary N atoms is important for enhancing the activity and stability of Pt/NG catalysts.

In contrast to N, P and B have lower electronegativity than carbon. However, P- or B-doped graphene materials exhibit similar good electrochemical performance—such as high conductivity and stability—to N-doped materials. The reason for the performance boost can be attributed to the presence of doped heteroatoms with different electronegativity, i.e., higher electron-donating ability that can break the electroneutrality of graphene to create charged sites, which further facilitates the deposition of Pt NPs and the ORR. However, the currently proposed mechanisms for the enhancement of Pt NP adsorption on heteroatom-doped carbon nanomaterials are very different [72]. Chen's team [72] showed that dopant nitrogen atoms in CNTs serve to mediate the enhancement in Pt adsorption by activating nitrogen-neighboring carbon atoms, due to large electron affinity of nitrogen. In contrast, the enhanced Pt adsorption in boron-doped CNTs can be mainly attributed to a strong hybridization between Pt d orbitals and boron p orbitals, leading to direct chemical bonding between the Pt and boron atoms. Musgrave's team [70] examined the doping mechanisms and effects of N- and B-doping on Pt atom adsorption and migration on graphene. There was a seemingly contradictory behavior between dopant type (n- vs. p-type) and charge accumulation on the dopant atoms: The N atoms in both n-type singly N-doped graphene (NG) and p-type triply N-doped graphene (3NG) gain electron density, while the B atoms in both singly (BG) and triply (3BG) B doped graphene are p-type and lose electron density. Therefore 3NG and N atoms form strong covalent bonds with the Pt atom, while in 3BG the B atoms form ionic bonds with the Pt atom.

In addition, when graphene is doped with elements having similar electronegativities to carbon (electronegativity of C: 2.55), such as sulfur (electronegativity of S: 2.58) and selenium (electronegativity of Se: 2.55), it also exhibits excellent catalytic activity and long-term stability [10, 73]. Higgins et al. [74] prepared sulfur-doped graphene (SG) by a thermal shock/quench annealing process, and investigated the activity and stability of Pt/SG for ORR. SG was found to be able to have a strong catalyst–support interaction, resulting in excellent half-cell based ORR activity of 139 $mA \cdot mg_{Pt}^{-1}$ at 0.9 V vs. RHE, a value significantly higher than the values of 121 $mA \cdot mg_{Pt}^{-1}$ reported for commercial Pt/C and 101 $mA \cdot mg_{Pt}^{-1}$ for Pt/G. Pt/SG also demonstrated unprecedented stability, maintaining 87% of its ECSA after accelerated degradation testing (ADT). Computational simulation highlighted that the interactions between Pt and graphene are enhanced significantly by S-doping, leading to a tethering effect that well explains the outstanding electrochemical stability.

3.4 Other novel carbon nanomaterials

Nanostructuring of support materials offers the possibility of controlling and improving several properties at the same time. Recently, several new nanostructured carbon supports, like hollow graphite spheres (HGS) [75], hollow carbon nanocages (CNCs) [76], ordered mesoporous carbon spheres (OMCS) [77], and carbon nano-onions (CNOs) [78], have been extensively studied. Unlike the one-dimensional (1D) and 2D carbon nanomaterials (carbon nanofibers (CNF), CNTs, graphene), these three-dimensional (3D) nanostructured carbon nanomaterials contain more interconnected

macropores and mesopores, which improve the electrocatalytic activity and long-term durability of the catalyst supported on them, as the porous structures form a large surface area for high dispersion of metal NPs, whilst simultaneously confining them inside the host. The excellent performance of 3D carbon materials was shown by Zhang et al. [77] who reported a 3D OMCS-supported Pt NPs (Pt/OMCS) catalyst. In Pt/OMCS, Pt NPs with mean size of ~1.6 nm were homogeneously dispersed on the mesopore walls of the carbon spheres. The Pt/OMCS catalyst exhibits larger ECSA, higher activity for the methanol oxidation reaction (MOR) and ORR, and better electrocatalyic stability than carbon black-supported Pt and commercial Pt/C catalysts. This shows that the unique hierarchical structures with ordered macropores and mesopores of OMCS not only facilitate the mass transfer giving increased accessibility to the active sites, but also make the Pt NPs less vulnerable to dissolution and aggregation than those supported on carbon black.

Galeano et al. [75] have proposed three key elements in the design of tailored mesoporous structure carbon supports, namely: (i) A high surface area (>1,000 $m^2 \cdot g^{-1}$) in order to provide good dispersion, (ii) a high degree of graphitization in order to reduce carbon corrosion issues, and (iii) an interconnected pore system with a narrow pore size distribution so that Pt nanoparticles can be encapsulated and thus stabilized. Based on the above key factors, they designed a mesostructured graphitic carbon support (Fig. 6(a)), HGS, with a specific surface area exceeding 1,000 $m^2 \cdot g^{-1}$ and precisely controlled pore structure. As shown in Figs. 6(b)–6(e), Pt NPs of approximately 3–4 nm size encapsulated in the HGS pore structure are stable even at 850 °C and, more importantly, during simulated ADT. The improved preservation of Pt surface area over the course of several thousand degradation cycles for the Pt@HGS materials can be explained in terms of the diminished detachment and agglomeration due to the confinement and good separation of the Pt NPs in the 3D mesopore system of the highly graphitic support.

Besides the special 3D structure of carbon nanomaterials, doping heteroatoms into carbon supports can also enhance the activity and stability of loaded metal NPs. Recently, Wang's team [76] described finding remarkably high durability by using a novel hollow carbon nanocage (CNC) material. The hollow CNCs have a high degree of graphitization and concurrent N-doping giving enhanced oxidation resistance, uniform deposition of fine Pt particles, and strong Pt–support interactions. ADT shows that the ECSA decreased from 68 to 34 $m^2 \cdot g^{-1}$ for Pt/CNC (1000) (by 50%), and from 46.4 to 7.82 $m^2 \cdot g^{-1}$ for a Johnson Matthey (JM) catalyst (by 83.2%) after 5,000 cycles (in the potential window from 0.6 to 1.24 V). Pt/CNC(1000) also shows superior electrochemical activity and long-term stability for both hydrogen oxidation and oxygen reduction, when compared to current industrial benchmark catalysts.

4 Noncarbon supports

Using more stable carbon materials, such as carbon nanotubes, graphene nanosheets, or carbon nanofibers, one would expect to alleviate the problems caused by the normal carbon black supports. However to date, none of the above investigated carbon materials have been able to completely prevent the electrochemical corrosion of carbon during extended operation and repeated cycling. Therefore, more robust and corrosion-resistant support materials need to be developed. Over the past few decades, numerous noncarbon catalyst supports, including transition metal oxides, transition metal nitrides, and transition metal carbides/borides, have been exhaustively researched due to their high corrosion resistance and strong metal–support interaction (SMSI).

4.1 Metal oxides

Various metal oxides/mixed oxides have been investigated as substitutes for carbon based FC catalysts, including SnO_2, TiO_2, WO_x, RuO_2, and SiO_2. Titanium oxide-based materials have garnered special attention because of their excellent corrosion resistance, cost-effectiveness, and nontoxicity. However, because of the lower electronic conductivity and surface area of metal oxides, a bare metal oxide supported catalyst is deemed unsuitable. However, doping such oxides with metals such as Zr, Hf, V, Nb, Mo, W, Os, and Sn has been found to increase their electronic conductivities and enlarge their surface areas.

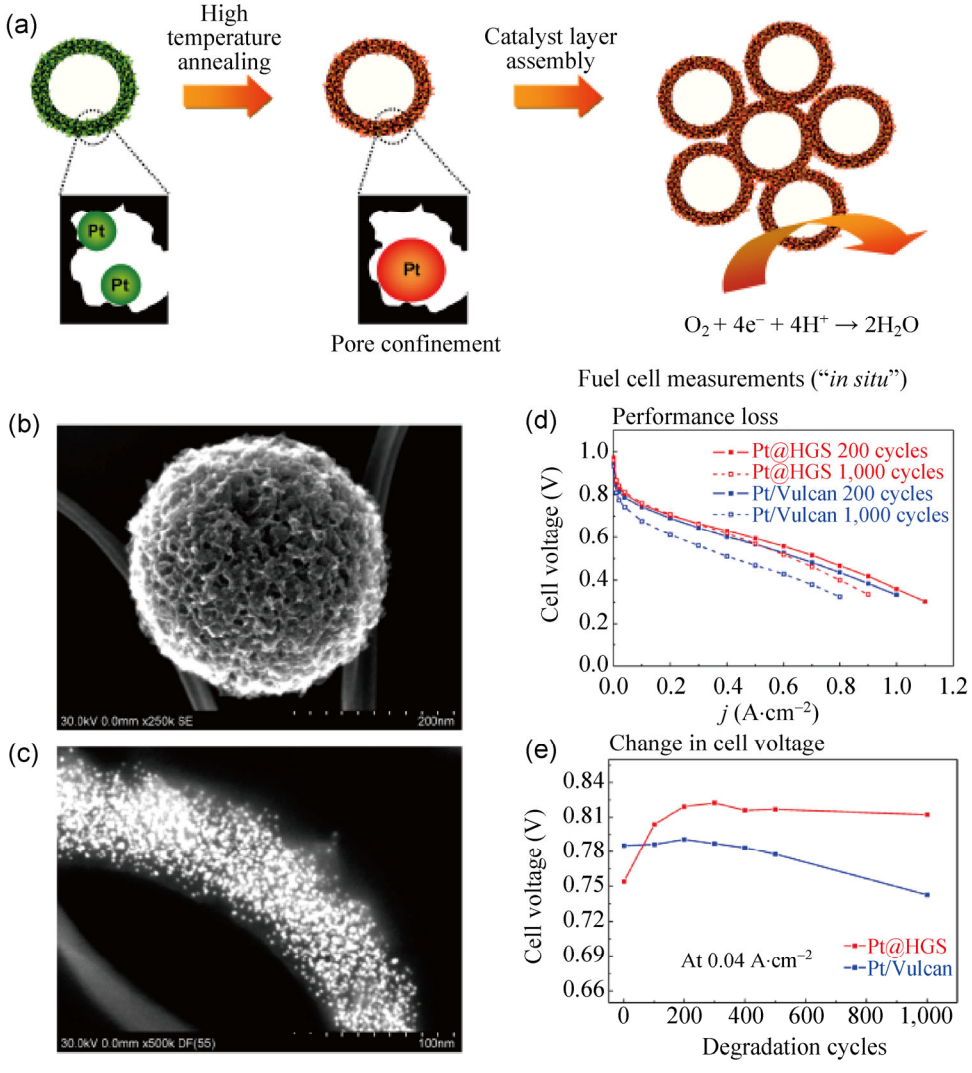

Figure 6 (a) Schematic mode of Pt encapsulation by pore confinement. (b) Representative high-resolution scanning electron micrograph of HGS support. (c) DF-STEM of a cross-sectional cutting of Pt@HGS (20 wt.%) after thermal treatment at 850 ˚C. (d) Fuel cell performance curves at 80 ˚C before and after degradation test under start-stop conditions. (e) Comparison of cell voltage change in the kinetic region for Pt@HGS and Pt/Vulcan during the *in situ* degradation tests at 0.04 A·cm^{-2} (with 0.18 and 0.36 mg_{Pt}·cm^{-2} loading at anode and cathode, respectively, for each catalyst). Reproduced with permission from Ref. [75], © American Chemical Society 2012.

Hwang's group [79] explored the use of robust non-carbon $Ti_{0.7}Mo_{0.3}O_2$ as a functionalized co-catalytic support for Pt/$Ti_{0.7}Mo_{0.3}O_2$. It features a high surface area (232 $m^2 \cdot g^{-1}$) and good electronic conductivity (2.8×10^{-4} S·cm^{-1}), as well as high stability in acidic solution and oxidative environments compared to TiO_2, MnO_2, and carbon black. In addition to the expected high activity, Pt/$Ti_{0.7}Mo_{0.3}O_2$ demonstrated extremely high stability, with no significant drop in activity after 5,000 cycles and only about 8% performance degradation at 0.9 V. Interestingly, Kumar and Ramani [80] reported an even higher activity and stability for a robust noncarbon $Ta_{0.3}Ti_{0.7}O_2$ supported Pt catalyst. The 20% Pt/$Ta_{0.3}Ti_{0.7}O_2$ catalysts were reported to be better in terms of all the measurements of ECSA, exchange current density, and mass activity than 20% Pt/C. After 10,000 cycles of a simulated start-up/shut down potential cycling AST (with the potential varying from 1.0 to 1.5 V vs. RHE at a scan rate of 500 mV·s^{-1}), the 20% Pt/$Ta_{0.3}Ti_{0.7}O_2$ catalyst exhibited exceptionally high electrochemical stability compared with both 20% Pt/C and a commercial 46% Pt/C (TKK) catalyst, and showed a loss of only 23 mV at 0.4 A·cm^{-2} compared with a loss of 330 and 340 mV

at the same current density, for the 20% Pt/C and TKK respectively. However, unlike the start–stop AST, exposure to the load cycling ADT (in the potential window from 0.6 to 0.95 V vs. RHE) had little impact on performance, confirming that the FC is far more forgiving of Pt dissolution than it is of support corrosion. The higher activity and stability of the 20% $Pt/Ta_{0.3}Ti_{0.7}O_2$ catalyst was attributed to the SMSI between Pt NPs and $Ta_{0.3}Ti_{0.7}O_2$, which resulted from electron donation from the $Ta_{0.3}Ti_{0.7}O_2$ support to the Pt atoms.

Recently, Wei's team [81, 82] developed an absolutely new metal oxide support—exfoliated montmorillonite (ex-MMT), which displays many attractive properties, such as high ion-exchange ability, high surface area, and a porous network structure. MMT is a crystalline 2:1 layered clay mineral, with a central alumina octahedral $Al(O,OH)_6$ sheet sandwiched between two silica tetrahedral SiO_4 nanoplatelets. A single triple-layer nanoplatelet, ex-MMT with a thickness of ~1 nm, can be exfoliated layer by layer from the repeat structure. The dangling bonds and ex-MMT nanoplatelets, which contain native defects plus newly created post-treatment defects, are very active for efficiently binding of foreign elements. Ding et al. showed [82] that the ex-MMT materials not only reinforce the metal–support interaction but also efficiently modify the electronic structures of metal NPs, thereby leading to enhanced activity and stability for ORR catalysis. For example, a Pd/ex-MMT catalyst exhibits very good ORR activity, which is much better than that of Pd/C, and indeed close to that of Pt/C. As shown in Figs. 7(a) and 7(b), after 800 cycles AST test (CV from 0 to 1.0 V in N_2-purged 0.1 M $HClO_4$), the activity of Pd/ex-MMT catalyst toward ORR exhibited no noticeable degradation. These results suggest that the Pd NPs were tightly anchored and stabilized on the ex-MMT nanoplatelets. First-principles calculations [81] revealed that ex-MMT has a defective structure with a strong anchoring ability for Pd NPs due to the formation of Pd–O–Al bonds (Fig. 7(c)), which further induces a thin PdO_x layer or Pd–O junction (Figs. 7(d)–7(g)). Because of the existence of the thin PdO_x layer or Pd–O junction, the Pd on the ex-MMT showed an electronic structure similar to that of Pt, thus exhibiting excellent catalytic activity for ORR. In addition, the defective or destroyed SiO_4 tetrahedra can be restructured directly by the O atoms from O_2 or indirectly by the intermediates formed by reduction of O_2.

4.2 Metal nitrides

Besides transition metal oxides, transition metal nitrides and transition metal carbides/borides, such as titanium nitride [83], titanium carbide [2, 84–86], boron carbide, silicon carbide, and titanium boride, have all received considerable attention due to their noble-metal-like catalytic properties, good electrical conductivity, and high resistance to corrosion and acid attack. Electrocatalysts using such materials as supports have been shown to have good catalytic activity and long-term durability.

Transition metal nitrides are an interesting class of materials for use as electrocatalyst supports since they are highly electrically conductive (metallic), thermally stable with high melting points, electrochemically stable under FC operation conditions, and exhibit exceptional hardness and corrosion resistance, as well as good catalyst–support interactions. Thus transition metal nitrides are able to afford electrocatalysts with high ORR activity and good electrochemical stability.

Avasarala et al. [87] compared the durability of Pt/TiN with that of Pt/C catalysts, and explained their degradation mechanism under FC conditions. Unlike Pt/C, the degradation of which involves a combination of Pt agglomeration and carbon support corrosion mechanisms, Pt/TiN degraded predominantly via a Pt agglomeration mechanism. This is because TiN has a higher resistance to corrosion than that of carbon under electrochemical conditions; as a result, the catalyst support corrosion mechanism plays a minor role in the degradation of Pt/TiN. In addition, they found that for the Pt/TiN catalyst, the Pt particle sizes became larger after ADT tests (compared to Pt/C), indicating a higher level of Pt agglomeration. To reduce the Pt agglomeration on TiN, they introduced a thin layer of oxynitride on Pt/TiN by annealing the latter material in nitrogen at controlled temperatures ranging between 70 and 120 °C. Unlike the oxide component which dissolved easily in the acidic electrolytes, the oxynitride showed stability for a longer period of time. The oxynitride layer grown on Pt/TiN partially encapsulates the catalyst particles, strongly binding them onto the

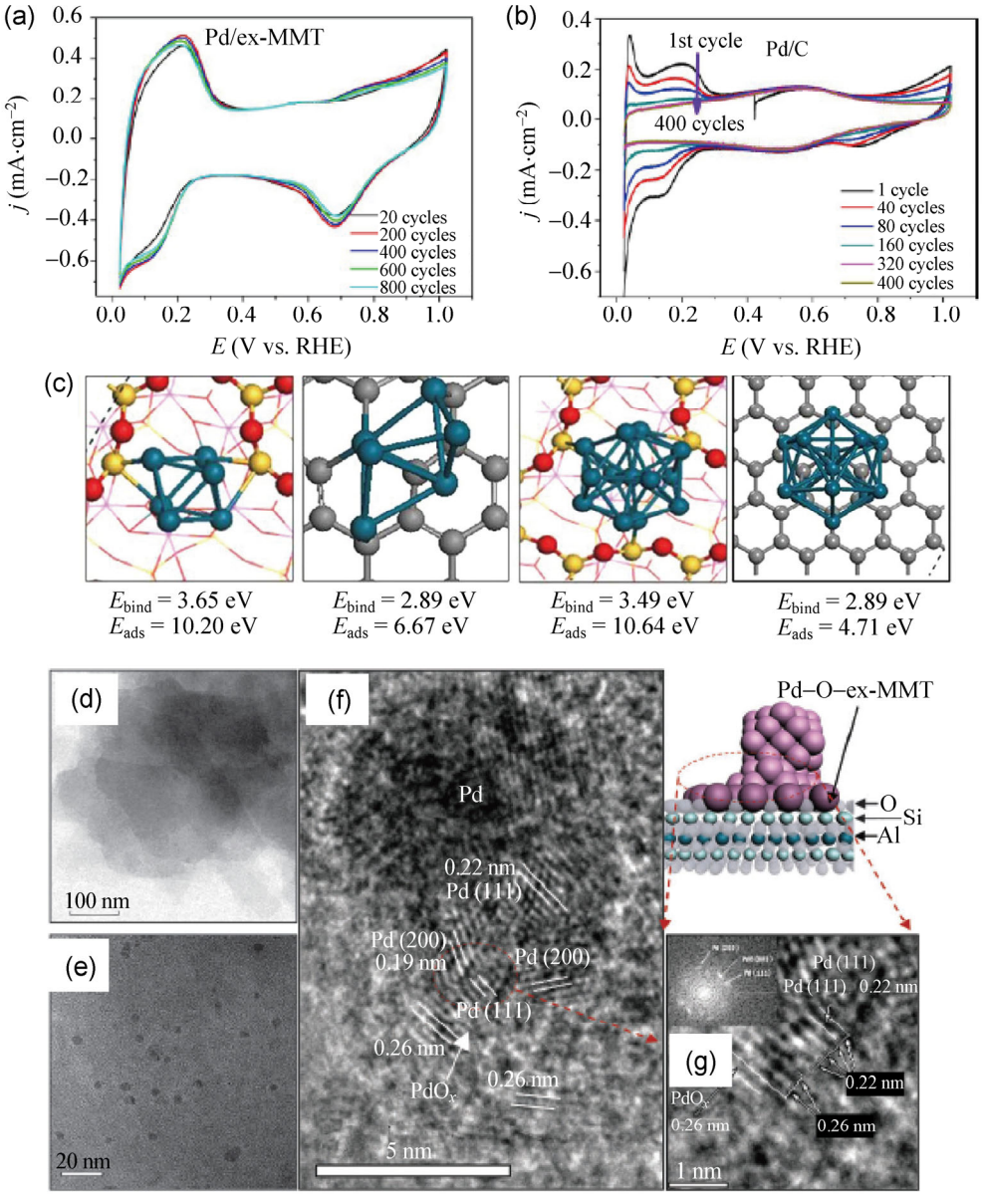

Figure 7 CV of (a) Pd/ex-MMT and (b) Pd/C in N_2 saturated 0.1 M $HClO_4$ solution using a 50 mV·s^{-1} scan rate. (c) Stable structures of Pd_n/MMT and Pd_n/graphene (n = 6, 13). (d) TEM of ex-MMT nanoplatelets. (e) TEM of the Pd/ex-MMT catalyst. (f) HRTEM of a typical Pd cluster on ex-MMT. (g) HRTEM and FFT of Pd–O–ex-MMT junctions. Reproduced with permission from Ref. [81], © American Chemical Society 2013, and Ref. [82], © the Royal Society of Chemistry 2014.

TiN support surface, and thereby limiting the Pt NPs mobility and agglomeration.

Pan et al. [15] developed hollow and porous TiN nanotubes (NTs) for supporting Pt NPs to enhance the activity and stability of an ORR catalyst. The mass activity and specific activity of Pt/TiN NTs were 0.4 A·mg$_{Pt}^{-1}$ and 0.87 mA·cm^{-2} (0.9 V vs. RHE), respectively, being around 2 and 2.9 times the values for a Pt/C (E-TEK) catalyst, respectively. The ADT test (in the potential window from 0.6 to 1.05 V in 0.5 M H_2SO_4 solution) revealed that the TiN support can dramatically enhance the durability of the catalyst and maintain the ECSA of Pt. After 12,000 cycles, the final ECSA of Pt/C (E-TEK) dropped to 71% of the initial value. However, the Pt/TiN showed an improvement in terms of ECSA loss, since 77% of the initial ECSA

remained after the same number of cycles. Besides the high corrosion resistance of TiN, the SMSI between Pt NPs and the TiN support is another factor enhancing the durability of Pt/TiN. The strong Pt–TiN interaction alters the electronic structure of the Pt NPs, which causes a shift of the Pt $4f_{7/2}$ peak to higher binding energy, thereby creating a stabilizing effect against Pt oxidation/dissolution. A strong Pt–TiN interaction is induced by the surface of the dendrite nanocrystal TiN, which may function as a "hunter" to recapture the re-nucleated Pt species dissolved in the electrolyte, thus effectively preventing the leaching and migration of dissolved Pt NPs.

Zhang et al. [88] used DFT calculations to investigate the interaction between Pt and the TiN surface. They found that atomic Pt does not bind well to the clean TiN surface under typical PEMFC operation conditions, i.e., strongly oxidizing conditions, and TiN surface vacancies play a crucial role in anchoring the Pt atom and enhancing its catalytic function. Specifically, when changing the conditions from N-lean to N-rich, the binding energy of Pt increased at the N vacancies, while decreasing at the Ti vacancies. Considering the energetic stability of the Pt/TiN structure for varying N contents, it was concluded that embedding Pt at the surface N-vacancy site is most favorable under N-lean conditions.

4.3 Metal carbides

Transition metal carbides have similar structures and physicochemical properties to their nitride counterparts. However, there are a couple of differences between carbides and nitrides, including the stoichiometry and coordination of the lattice, which is dictated by the stable oxidation state for C (–4) compared to N (–3), and the magnitude of electron transfer between the adatom and metal, since C has a significantly smaller electronegativity than N. For example, in the case of titanium-based materials, the Ti binding energy might shift to a lower value on going from TiN to TiC, because the electropositivity of Ti is lower in TiC than that in TiN. Consequently Pt reduction is favored for the former [26, 84].

Carbide-based electrocatalysts are highly active for both the ORR and alcohol oxidation. However, a crucial problem that remains unsolved is the stability of the carbides. Roca-Ayats et al. [84] compared the electrocatalytic stability of Pt_3Ir NPs supported on TiC, TiCN, and TiN for ORR. They found that the Pt_3Ir/TiC catalyst had the worst performance and stability, while Pt_3Ir/TiCN showed the highest activity toward ORR, and Pt_3Ir/TiN had the best compromise between catalytic activity and stability. In order to simultaneously get best activity and stability, Ma's team [89] explored a new *in situ* ion-exchange method by which one can stabilize carbide-based materials through synthesizing bimetallic carbide nanocomposites ($Co_6Mo_6C_2$/C). As-obtained Pt/$Co_6Mo_6C_2$/C catalysts showed both superior activity and high stability in comparison with Pt/C. The Pt/$Co_6Mo_6C_2$/C catalyst had a mass activity of 271.7 $A \cdot g_{Pt}^{-1}$ at 0.9 V for ORR, which is 2.5 times higher than that of Pt/C (108.6 $A \cdot g_{Pt}^{-1}$). The better performance of the Pt/$Co_6Mo_6C_2$/C catalyst can be explained by the synergistic effect between the $Co_6Mo_6C_2$/C support and the active Pt NPs. At the same time, the higher mass activity of Pt/$Co_6Mo_6C_2$/C indicated that it is possible to use a significantly reduced amount of noble metal Pt to reach the same performance, and lower the cost of the FC. After 1,000 cycles of ADT testing (in the potential window from 0.05 to 1.1 V vs. RHE), there was no observable loss of ECSA for Pt/$Co_6Mo_6C_2$/C, while ~20% loss of ECSA was observed for Pt/C. The improved stability might originate from the much higher stability of $Co_6Mo_6C_2$/C compared to carbon under the test conditions.

Quite recently, Wei's group [90, 91] developed surface Al leached Ti_3AlC_2 particles (e-TAC) with high corrosion resistance and excellent electrical conductivity as an advanced support material for Pt catalysts, as shown in Fig. 8. Ti_3AlC_2, belonging to a large family of layered hexagonal ternary metal carbides referred to as MAX phases, has high chemical stability and good electrical conductivity. However, nanosized Ti_3AlC_2 lacks sufficient binding sites to anchor Pt NPs due to its low surface area and the chemical inertness of the material surface, which may lead to poor Pt dispersion and large Pt NPs. These problems were solved by using an optimized hydrothermal etching method (Fig. 8(a)), leading to a well-structured and well-functionalized Ti_3AlC_2 support material. Electrochemical measurements confirmed that the supported Pt/e-TAC electrocatalyst shows much improved activity

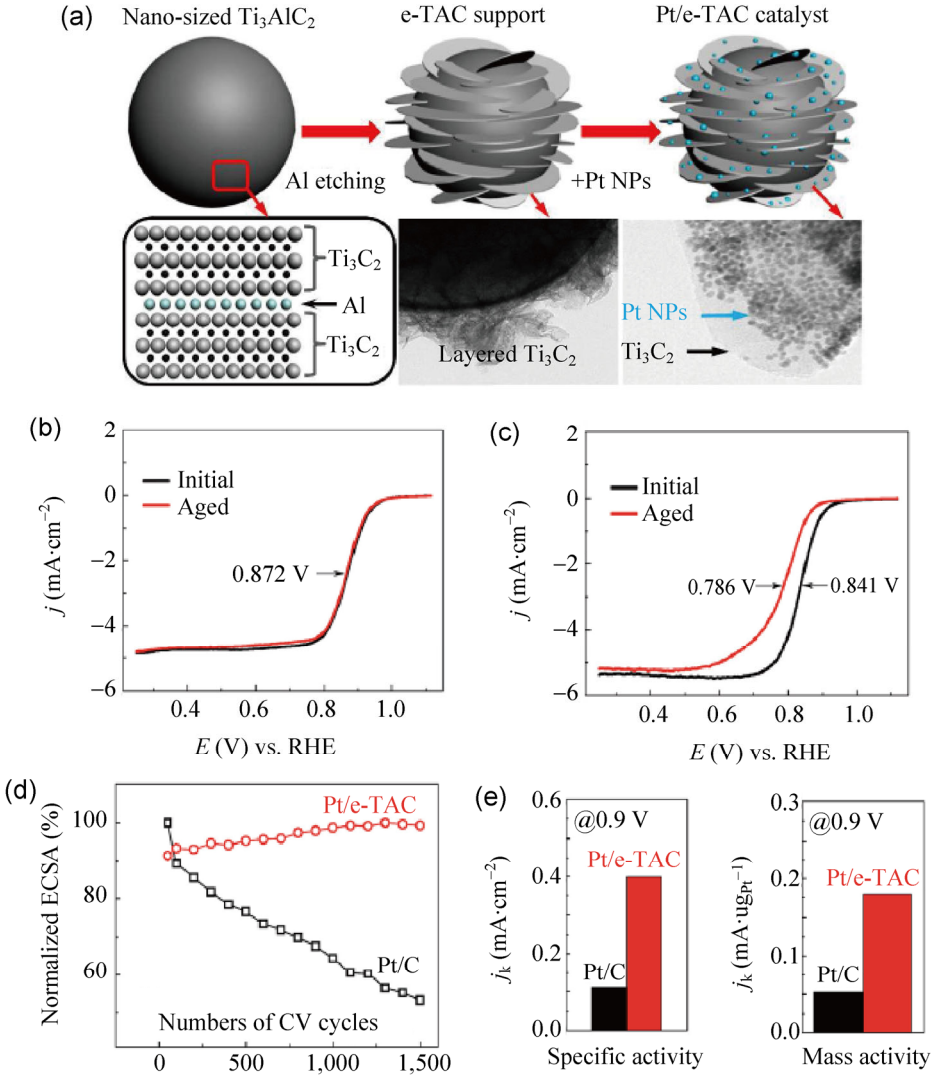

Figure 8 (a) Schematic of Pt/e-TAC catalyst formation. ORR polarization curves for (b) Pt/e-TAC and (c) Pt/C catalysts before and after ADT cycling (recorded in O_2-saturated 0.1 M $HClO_4$ at 1,600 rpm and with a scan rate of 10 mV·s^{-1}). (d) Normalization Pt ECSA of Pt/e-TAC and Pt/C catalysts as a function of the number of CV cycles. Pt loading for both electrodes is about 10 μg. (e) Specific activity and mass activity at 0.9 V for Pt/e-TAC and Pt/C catalysts. Reproduced with permission from Ref. [90], © the Royal Society of Chemistry 2013, and Ref. [91], © the Royal Society of Chemistry 2014.

and enhanced durability toward ORR when compared with a commercial Pt/C catalyst. The BET surface area of the e-TAC (10.35 $m^2 \cdot g^{-1}$) was approximately 10 times higher than that of pristine Ti_3AlC_2 (1.18 $m^2 \cdot g^{-1}$). The electrical conductivity of e-TAC (4.3×10^{-2} S·cm^{-1}) was comparable to carbon black (2.4×10^{-1} S·cm^{-1}), but significantly higher than the conductivity of commercial TiO_2. The initial specific ECSA based on the Pt mass for Pt/e-TAC (44.81 $m^2 \cdot g^{-1}$) was found to be similar to that of the Pt/C catalyst (47.05 $m^2 \cdot g^{-1}$). As shown in Fig. 8(e), the specific activity of the Pt/e-TAC catalyst is three times greater than that of the Pt/C catalyst. Similarly, the mass activity of the Pt/e-TAC (0.180 A·mg$_{Pt}^{-1}$) is also three times greater than that of Pt/C (0.0518 A·mg$_{Pt}^{-1}$). After 1,500 cycles of ADT tests (in the potential window from 0.0 to 1.2 V vs. RHE in 0.1 M N_2-saturated $HClO_4$), a considerable ECSA loss (approximately 48%) was observed for Pt/C (Figs. 8(b)–8(d)). In contrast, in the case of Pt/e-TAC, it is important to highlight that the normalized ECSA of Pt/e-TAC kept increasing slightly during the ADT cycling, indicating that the stability of the

Pt/e-TAC is far superior to that of Pt/C. DFT calculations revealed that the formation of Pt–Ti bonds and the electron transfer between the Pt d states and the Ti d states resulted in a stronger interaction between the Ti_3C_2 and the Pt NPs. Such a strong interaction makes the Pt NPs spread out on the Ti_3C_2 support.

5 Hybrid supports

As mentioned above, non-carbon supports, such as metal oxides and metal nitride/carbides greatly improve the stability of FC catalysts due to the high corrosion resistance and SMSI. However, compared to carbon supports, some drawbacks of noncarbon supports such as low electronic conductivity, large solubility, insufficient chemical/electrochemical, and thermal stability, as well as low surface area, have been found to hinder their actual application as catalyst supports. To overcome the above barriers, hybrid supports [16, 92], which are composed of the different carbon supports (graphene–CB, graphene–CNTs, SWCNTs–MWCNTs) [93, 94] or combined noncarbon and carbon supports such as SnO_2–CNTs [49], TiO_2–CNTs [51], IrO_2–CNTs [52], $TaNbTiO_2$–C [95], and ITO (indium tin oxide)–graphene [96] have been considered as promising catalyst supports for the FC electrocatalyst application.

Huang's team [93] inserted carbon black (CB) particles between Pt/reduced graphene oxide (RGO) sheets in an attempt to prevent the stacking of RGO sheets and enhance the electron-transfer rate both in the graphene sheets, and across the Pt NPs–RGO interface. Interestingly, they found that the well-mixed RGO/CB composite structure not only enhances the catalytic activity but also dramatically improves the durability of the catalyst. The ADT showed that the final ECSA of the Pt NPs on the hybrid RGO/CB support after 20,000 ADT cycles was >95% of the original value, much higher than for the commercially available catalyst. TEM observation combined with electrochemical measurements suggested that, in the hybrid structure, the flexible 2D profile of RGO may function as a "mesh" that prevents leaching of dissolved Pt species into the electrolyte, while the CBs can serve as active sites for recapture or renucleation of small Pt clusters.

Wang's team [51] reported a high-stability Pt catalyst support involving hierarchical CNTs@TiO_2 structures composed of TiO_2 nanosheets grafted on a CNT backbone, as shown in Fig. 9. The Pt/CNT@TiO_2 catalyst showed high electrocatalytic activity, with greatly improved stability compared to conventional CNT or CB-supported Pt catalysts. After 5,000 cycles of ADT testing, the ECSA of Pt/CNT@TiO_2 was 78% of the original value, while the ECSA of Pt/CNT and Pt/CB only retained 57% and 9%, respectively, of their original values (Figs. 9(b) and 9(c)). The high electrocatalytic activity and ultrahigh stability of Pt/CNT@TiO_2 were ascribed to a synergetic effect of CNT and TiO_2. In this CNT@TiO_2 structure, the "hairy" TiO_2 decorated on the surface of CNTs with a well-developed mesoporous structure not only prevents the aggregation of Pt NPs due to the SMSI, but also provides channels for rapid mass transfer. In addition, the high conductivity of the CNT backbone favors rapid electron transfer.

Recently, Wang et al. [95] synthesized a novel hybrid support—a C–$TaNbTiO_2$ support—which was employed as a carbon substitute supports for PtPd alloy catalysts for ORR. Compared to pure carbon or $TaNbTiO_2$ supports, the C–$TaNbTiO_2$ hybrid support had a high specific surface area, favoring the uniform distribution of PtPd alloy NPs, and sufficient electronic conductivity for electron transfer between the PtPd alloy NPs and the support in the ORR. PtPd/C–$TaNbTiO_2$ exhibited higher activity, better ORR durability, and a limited ORR loss of 30%, values which are all lower than those for 40% Pt/C (TKKE). The activity and durability improvement was attributed to a strong physico-chemical interaction between catalyst metal NPs, carbon–$TaNbTiO_2$ support and carbon, as well as the stability of the oxide protecting the carbon from corrosion by the distribution of the oxide on the carbon.

6 Summary and outlook

We have presented a short review of recent research and developments in enhancing the long-term durability of supported Pt-based catalysts. Corrosion of the carbon support and Pt dissolution are believed to be the major primary degradation mechanisms.

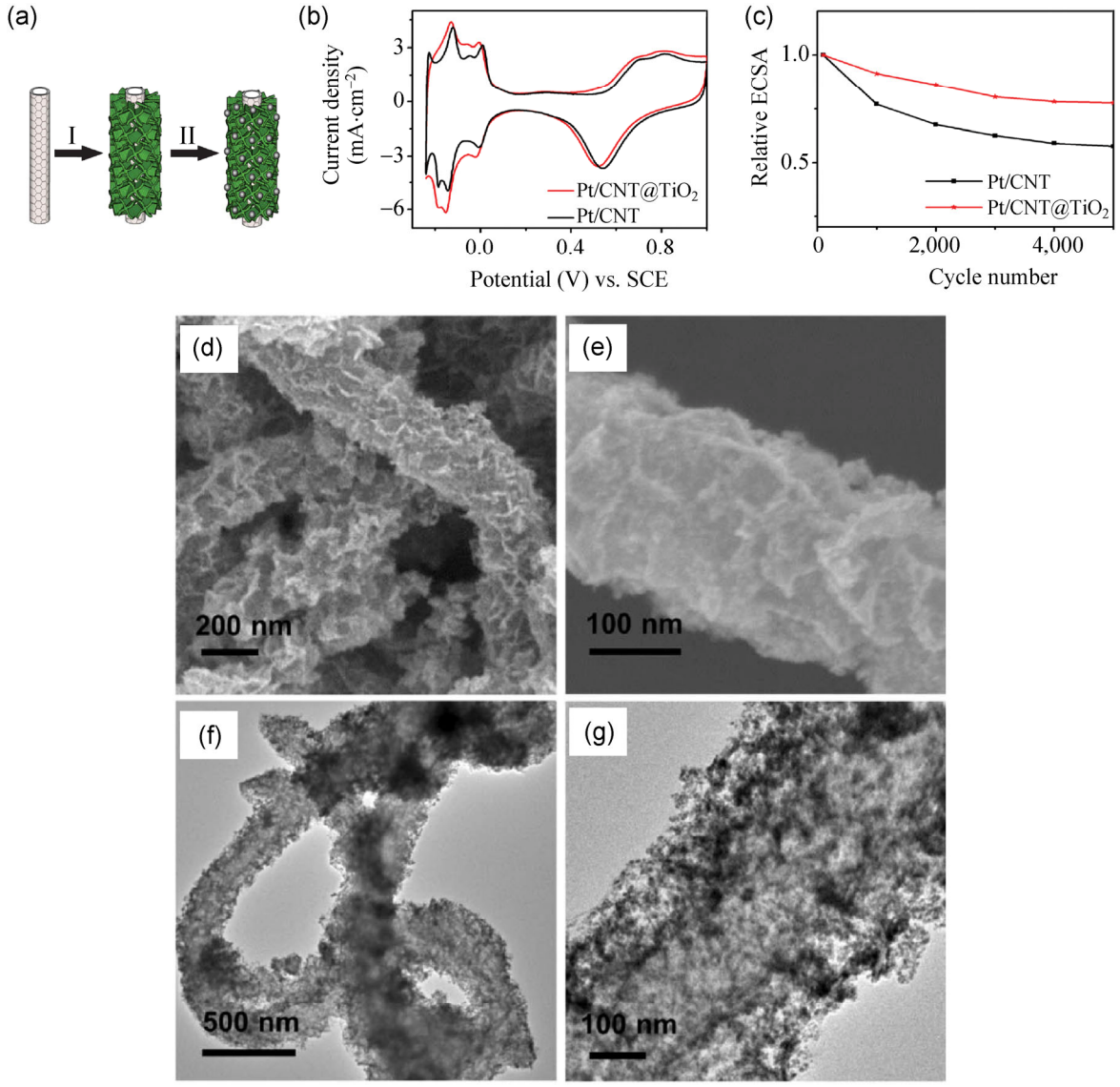

Figure 9 (a) Schematic illustration of the Pt/CNT@TiO_2 preparation process. (b) CV of Pt/CNT and Pt/CNT@TiO_2, in which the Pt loading on the electrode is 0.2 mg·cm^{-2}, and the potential sweep rate is 20 mV·s^{-1}. (c) The normalized ECSA plots for the Pt/CNT and Pt/CNT@TiO_2 catalysts. (d) and (e) SEM and (f) and (g) TEM images of Pt/CNT@TiO_2 catalyst. Reproduced with permission from Ref. [51], © the Royal Society of Chemistry 2011.

Thus, searching for supports with high stability, enhancing the oxidation resistance of Pt NPs, and increasing the interaction between the Pt NPs and supports are all critical targets for attaining improved durability. The design of Pt-based alloy NPs with different surfaces, and substituting carbon black supports with novel support materials having high electrical conductivity, high surface area, and excellent electrochemical durability are the most widely used approaches.

Novel carbon nanomaterials such as CNTs, graphene, and nanoporous carbon, which offer the advantages of large surface area, high electrical conductivity, and excellent electrochemical durability, are the most promising supports. However, the high graphitization degree of these novel carbon nanomaterials leads to weak interactions with Pt NPs and fewer anchoring sites. Thus, the design of new linkers between metal NPs and novel carbon nanomaterial supports provides a promising solution for the future development of

high stability Pt-based catalysts for FC and other energy device applications.

Noncarbon supports—including transition metal carbides/borides and transition metal oxides—have high corrosion resistance and SMSI which makes them excellent candidates for supports. The catalytic activity and stability of noncarbon supported Pt-based catalysts strongly depends on the conductivity and the structure of the supports. Therefore, it is important to carefully tailor the fabrication methods in order to increase the surface area and electrical conductivity.

To improve the durability of Pt-based catalysts, different kinds of supports have been combined in hybrid supports. Whether obtained by mixing carbon supports with noncarbon supports, or merging different carbon nanomaterials together, the hybrid supports generally exhibit higher performance in terms of activity and stability than the parent supports. Thus, such hybrid supports must be considered as promising catalyst supports for FC catalyst applications.

Acknowledgements

Our research was financially sponsored by National Basic Research Program of China (Grant Nos. 2012CB215500 and 2012CB720300) and the National Natural Science Foundation of China (Grant Nos. 20936008, 21176271, 21276291, 21376284, and 21436003).

References

[1] Sharma, S.; Pollet, B. G. Support materials for PEMFC and DMFC electrocatalysts—A review. *J. Power Sources* **2012**, *208*, 96–119.

[2] Zhao, Y.; Wang, Y.; Cheng, X.; Dong, L.; Zhang, Y.; Zang, J. Platinum nanoparticles supported on epitaxial TiC/nanodiamond as an electrocatalyst with enhanced durability for fuel cells. *Carbon* **2014**, *67*, 409–416.

[3] U.S. Departement of Energy. Fuel cell technical team roadmap. 2013. http://energy.gov/sites/prod/files/2014/02/f8/fctt_roadmap_june2013.pdf.

[4] Sun, X.; Li, D.; Ding, Y.; Zhu, W.; Guo, S.; Wang, Z. L.; Sun, S. Core/shell Au/CuPt nanoparticles and their dual electrocatalysis for both reduction and oxidation reactions. *J. Am. Chem. Soc.* **2014**, *136*, 5745–5749.

[5] Su, L.; Jia, W. Z.; Li, C. M.; Lei, Y. Mechanisms for enhanced performance of platinum-based electrocatalysts in proton exchange membrane fuel cells. *ChemSusChem* **2014**, *7*, 361–378.

[6] Marcu, A.; Toth, G.; Pietrasz, P.; Waldecker, J. Cathode catalysts degradation mechanism from liquid electrolyte to membrane electrode assembly. *C. R. Chimie.* **2014**, *17*, 752–759.

[7] Takenaka, S.; Miyamoto, H.; Utsunomiya, Y.; Matsune, H.; Kishida, M. Catalytic activity of highly durable Pt/CNT catalysts covered with hydrophobic silica layers for the oxygen reduction reaction in PEFCs. *J. Phys. Chem. C* **2014**, *118*, 774–783.

[8] Kuo, P. L.; Hsu, C. H.; Wu, H. M.; Hsu, W. S.; Kuo, D. Controllable-nitrogen doped carbon layer surrounding carbon nanotubes as novel carbon support for oxygen reduction reaction. *Fuel Cells* **2012**, *12*, 649–655.

[9] Zhou, X.; Qiao, J.; Yang, L.; Zhang, J. A review of graphene-based nanostructural materials for both catalyst supports and metal-free catalysts in PEM fuel cell oxygen reduction reactions. *Adv. Energy Mater.* **2014**, *4*, 1301523.

[10] Park, J. E.; Jang, Y. J.; Kim, Y. J.; Song, M. S.; Yoon, S.; Kim, D. H.; Kim, S. J. Sulfur-doped graphene as a potential alternative metal-free electrocatalyst and Pt-catalyst supporting material for oxygen reduction reaction. *Phys. Chem. Chem. Phys.* **2014**, *16*, 103–109.

[11] Wang, S.; Zhang, L.; Xia, Z.; Roy, A.; Chang, D. W.; Baek, J. B.; Dai, L. BCN graphene as efficient metal-free electrocatalyst for the oxygen reduction reaction. *Angew. Chem. Int. Edit.* **2012**, *51*, 4209–4212.

[12] Wang, X.; Chen, Z.; Wang, Y.; Wang, R. Rare-earth-doped Pt/Ba/$Ce_{0.6}Zr_{0.4}O_2$–Al_2O_3 for NO_x storage and reduction: The effect of rare-earth doping on efficiency and stability. *ChemCatChem* **2014**, *6*, 237–244.

[13] Danilovic, N.; Subbaraman, R.; Chang, K. C.; Chang, S. H.; Kang, Y. J.; Snyder, J.; Paulikas, A. P.; Strmcnik, D.; Kim, Y. T.; Myers, D.; Stamenkovic, V. R.; Markovic, N. M. Activity–stability trends for the oxygen evolution reaction on monometallic oxides in acidic environments. *J. Phys. Chem. Lett.* **2014**, *5*, 2474–2478.

[14] Tripković, V.; Abild-Pedersen, F.; Studt, F. Cerri, I.; Nagami, T.; Bligaard, T.; Rossmeisl, J. Metal oxide-supported platinum overlayers as proton-exchange membrane fuel cell cathodes. *ChemCatChem* **2012**, *4*, 228–235.

[15] Pan, Z.; Xiao, Y.; Fu, Z.; Zhan, G.; Wu, S.; Xiao, C.; Hu, G.; Wei, Z. Hollow and porous titanium nitride nanotubes as high-performance catalyst supports for oxygen reduction reaction. *J. Mater. Chem. A* **2014**, *2*, 13966–13975.

[16] Yin, J.; Wang, L.; Tian, C.; Tan, T.; Mu, G.; Zhao, L.; Fu, H. Low-Pt loaded on a vanadium nitride/graphitic carbon

composite as an efficient electrocatalyst for the oxygen reduction reaction. *Chem. -Eur. J.* **2013**, *19*, 13979–13986.

[17] Liu, X.; Fu, G.; Chen, Y.; Tang, Y.; She, P.; Lu, T. Pt–Pd–Co trimetallic alloy network nanostructures with superior electrocatalytic activity towards the oxygen reduction reaction. *Chem. -Eur. J.* **2014**, *20*, 585–590.

[18] Mathias, M. F.; Makharia, R.; Gasteiger, H. A.; Conley, J. J.; Fuller, T. J.; Gittleman, C. J.; Kocha, S. S.; Miller, D. P.; Mittelsteadt, C. K.; et al. Two fuel cell cars in every garage. *Electrochem. Soc. Interface* **2005**, *3*, 24–35.

[19] Makharia, R.; Kocha, S.; Yu, P.; Sweikart, M. A.; Gu, W.; Wagner, F.; Gasteiger, H. A. Durable PEM fuel cell electrode materials: Requirements and benchmarking methodologies. *ECS Trans.* **2006**, *1*, 3–18.

[20] Zhang, Y.; Chen, S.; Wang, Y.; Ding, W.; Wu, R.; Li, L.; Qi, X.; Wei, Z. Study of the degradation mechanisms of carbon-supported platinum fuel cells catalyst via different accelerated stress test. *J. Power Sources* **2015**, *273*, 62–69.

[21] Chen, S.; Wei, Z.; Qi, X.; Dong, L.; Guo, Y. G.; Wan, L.; Shao, Z.; Li, L. Nanostructured polyaniline-decorated Pt/C@PANI core–shell catalyst with enhanced durability and activity. *J. Am. Chem. Soc.* **2012**, *134*, 13252–13255.

[22] Carpenter, M. K.; Moylan, T. E.; Kukreja, R. S.; Atwan, M. H.; Tessema, M. M. Solvothermal synthesis of platinum alloy nanoparticles for oxygen reduction electrocatalysis. *J. Am. Chem. Soc.* **2012**, *134*, 8535–8542.

[23] Wang, X.; Li, W.; Chen, Z.; Waje, M.; Yan, Y. Durability investigation of carbon nanotube as catalyst support for proton exchange membrane fuel cell. *J. Power Sources* **2006**, *158*, 154–159.

[24] Saleh, F. S.; Easton, E. B. Diagnosing degradation within PEM Fuel cell catalyst layers using electrochemical impedance spectroscopy. *J. Electrochem. Soc.* **2012**, *159*, B546–B553.

[25] Dubau, L.; Castanheira, L.; Maillard, F.; Chatenet, M.; Lottin, O.; Maranzana, G.; Dillet, J.; Lamibrac, A.; Perrin, J. C.; Moukheiber, E.; et al. A review of PEM fuel cell durability: Materials degradation, local heterogeneities of aging and possible mitigation strategies. *WIREs: Energy Environ.* **2014**, *3*, 540–560.

[26] Shrestha, S.; Liu, Y.; Mustain, W. E. Electrocatalytic activity and stability of Pt clusters on state-of-the-art supports: A review. *Catal. Rev.* **2011**, *53*, 256–336.

[27] Li, L.; Chen, S. G.; Wei, Z. D.; Qi, X. Q.; Xia, M. R.; Wang, Y. Q. Experimental and DFT study of thiol-stabilized Pt/CNTs catalysts. *Phys. Chem. Chem. Phys.* **2012**, *14*, 16581–16587.

[28] Shao, Y.; Yin, G.; Gao, Y.; Shi, P. Durability study of Pt/C and Pt/CNTs catalysts under simulated PEM fuel cell conditions. *J. Electrochem. Soc.* **2006**, *153*, A1093–A1097.

[29] Meier, J. C.; Galeano, C.; Katsounaros, I.; Topalov, A. A.; Kostka, A.; Schüth, F.; Mayrhofer, K. J. J. Degradation mechanisms of Pt/C fuel cell catalysts under simulated start–stop conditions. *ACS Catal.* **2012**, *2*, 832–843.

[30] Yu, X. W.; Ye, S. Y. Recent advances in activity and durability enhancement of Pt/C catalytic cathode in PEMFC: Part I. Physico-chemical and electronic interaction between Pt and carbon support, and activity enhancement of Pt/C catalyst. *J. Power Sources* **2007**, *172*, 133–144.

[31] Gilbert, J. A.; Kariuki, N. N.; Subbaraman, R.; Kropf, A. J.; Smith, M. C.; Holby, E. F.; Morgan, D.; Myers, D. J. *In situ* anomalous small-angle X-ray scattering studies of platinum nanoparticle fuel cell electrocatalyst degradation. *J. Am. Chem. Soc.* **2012**, *134*, 14823–14833.

[32] Fayette, M.; Nutariya, J.; Vasiljevic, N.; Dimitrov, N. A study of Pt dissolution during formic acid oxidation. *ACS Catal.* **2013**, *3*, 1709–1718.

[33] Topalov, A. A.; Katsounaros, I.; Auinger, M.; Cherevko, S.; Meier, J. C.; Klemm, S. O.; Mayrhofer, K. J. J. Dissolution of platinum: Limits for the deployment of electrochemical energy conversion? *Angew. Chem. Int. Edit.* **2012**, *51*, 12613–12615.

[34] Umeda, M.; Kuwahara, Y.; Nakazawa, A.; Inoue, M. Pt degradation mechanism in concentrated sulfuric acid studied using rotating ring-disk electrode and electrochemical quartz crystal microbalance. *J. Phys. Chem. C* **2009**, *113*, 15707–15713.

[35] Tang, L.; Han, B.; Persson, K.; Friesen, C.; He, T.; Sieradzki, K.; Ceder, G. Electrochemical stability of nanometer-scale Pt particles in acidic environments. *J. Am. Chem. Soc.* **2009**, *132*, 596–600.

[36] Noël, J. M.; Yu, Y.; Mirkin, M. V. Dissolution of Pt at moderately negative potentials during oxygen reduction in water and organic media. *Langmuir* **2013**, *29*, 1346–1350.

[37] Ishimoto, T.; Ogura, T.; Umeda, M.; Koyama, M. Theoretical study on dissolution and reprecipitation mechanism of Pt complex in Pt electrocatalyst. *J. Phys. Chem. C* **2011**, *115*, 3136–3142.

[38] Merte, L. R.; Behafarid, F.; Miller, D. J.; Friebel, D.; Cho, S.; Mbuga, F.; Sokaras, D.; Alonso-Mori, R.; Weng, T. C.; Nordlund, D.; et al. Electrochemical oxidation of size-selected Pt nanoparticles studied using *in situ* high-energy-resolution X-ray absorption spectroscopy. *ACS Catal.* **2012**, *2*, 2371–2376.

[39] Rinaldo, S. G.; Stumper, J. R.; Eikerling, M. Physical theory of platinum nanoparticle dissolution in polymer electrolyte fuel cells. *J. Phys. Chem. C* **2010**, *114*, 5773–5785.

[40] Tang, L.; Li, X.; Cammarata, R. C.; Friesen, C.; Sieradzki, K.

Electrochemical stability of elemental metal nanoparticles. *J. Am. Chem. Soc.* **2010**, *132*, 11722–11726.

[41] Hansen, T. W.; DeLaRiva, A. T.; Challa, S. R.; Datye, A. K. Sintering of catalytic nanoparticles: Particle migration or Ostwald ripening? *Acc. Chem. Res.* **2013**, *46*, 1720–1730.

[42] Yoshida, K.; Bright, A.; Tanaka, N. Direct observation of the initial process of Ostwald ripening using spherical aberration-corrected transmission electron microscopy. *J. Electron Microsc.* **2012**, *61*, 99–103.

[43] Hoogers, G. *Fuel Cell Technology Handbook*; CRC Press: New York, 2002.

[44] Speder, J.; Zana, A.; Spanos, I.; Kirkensgaard, J. J. K.; Mortensen, K.; Hanzlik, M.; Arenz, M. Comparative degradation study of carbon supported proton exchange membrane fuel cell electrocatalysts—The influence of the platinum to carbon ratio on the degradation rate. *J. Power Sources* **2014**, *261*, 14–22.

[45] Wang, J.; Yin, G.; Shao, Y.; Zhang, S.; Wang, Z.; Gao, Y. Effect of carbon black support corrosion on the durability of Pt/C catalyst. *J. Power Sources* **2007**, *171*, 331–339.

[46] Li, L.; Xue, Y.; Xia, M. R.; Chen, S. G.; Wei, Z. D. Density functional theory study of electronic structure and catalytic activity for Pt/C catalyst covered by polyaniline. *Scientia Sinica Chimica* **2013**, *43*, 1566–1577.

[47] Higgins, D. C.; Meza, D.; Chen, Z. Nitrogen-doped carbon nanotubes as platinum catalyst supports for oxygen reduction reaction in proton exchange membrane fuel cells. *J. Phys. Chem. C* **2010**, *114*, 21982–21988.

[48] Takenaka, S.; Matsumori, H.; Nakagawa, K.; Matsune, H.; Tanabe, E.; Kishida, M. Improvement in the durability of Pt electrocatalysts by coverage with silica layers. *J. Phys. Chem. C* **2007**, *111*, 15133–15136.

[49] Du, C.; Chen, M.; Cao, X.; Yin, G.; Shi, P. A novel CNT@SnO_2 core–sheath nanocomposite as a stabilizing support for catalysts of proton exchange membrane fuel cells. *Electrochem. Commun.* **2009**, *11*, 496–498.

[50] Masa, J.; Bordoloi, A.; Muhler, M.; Schuhmann, W.; Xia, W. Enhanced electrocatalytic stability of platinum nanoparticles supported on a nitrogen-doped composite of carbon nanotubes and mesoporous titania under oxygen reduction conditions. *ChemSusChem* **2012**, *5*, 523–525.

[51] Xia, B. Y.; Ding, S.; Wu, H. B.; Wang, X.; Wen, X. Hierarchically structured Pt/CNT@TiO_2 nanocatalysts with ultrahigh stability for low-temperature fuel cells. *Rsc. Adv.* **2012**, *2*, 792–796.

[52] Wang, H.; Zheng, J.; Peng, F.; Yu, H. Pt/IrO_2/CNT anode catalyst with high performance for direct methanol fuel cells. *Catal. Commun.* **2013**, *33*, 34–37.

[53] Chen, S.; Wei, Z.; Guo, L.; Ding, W.; Dong, L.; Shen, P.; Qi, X.; Li, L. Enhanced dispersion and durability of Pt nanoparticles on a thiolated CNT support. *Chem. Commun.* **2011**, *47*, 10984–10986.

[54] Kim, Y. T.; Mitani, T. Surface thiolation of carbon nanotubes as supports: A promising route for the high dispersion of Pt nanoparticles for electrocatalysts. *J. Catal.* **2006**, *238*, 394–401.

[55] Park, S. A.; Kim, D. S.; Kim, T. J.; Kim, Y. T. Strong interaction between Pt and thiolated carbon for electrocatalytic durability enhancement. *ACS Catal.* **2013**, *3*, 3067–3074.

[56] Hsu, C. H.; Liao, H. Y.; Kuo, P. L. Aniline as a dispersant and stabilizer for the preparation of Pt nanoparticles deposited on carbon nanotubes. *J. Phys. Chem. C* **2010**, *114*, 7933–7939.

[57] Wang, S.; Yu, D.; Dai, L. Polyelectrolyte functionalized carbon nanotubes as efficient metal-free electrocatalysts for oxygen reduction. *J. Am. Chem. Soc.* **2011**, *133*, 5182–5185.

[58] He, D.; Zeng, C.; Xu, C.; Cheng, N.; Li, H.; Mu, S.; Pan, M. Polyaniline-functionalized carbon nanotube supported platinum catalysts. *Langmuir* **2011**, *27*, 5582–5588.

[59] Guo, S.; Dong, S.; Wang, E. Constructing carbon nanotube/Pt nanoparticle hybrids using an imidazolium-salt-based ionic liquid as a linker. *Adv. Mater.* **2010**, *22*, 1269–1272.

[60] Fujigaya, T.; Nakashima, N. Fuel cell electrocatalyst using polybenzimidazole-modified carbon nanotubes as support materials. *Adv. Mater.* **2013**, *25*, 1666–1681.

[61] Guo, S.; Sun, S. FePt nanoparticles assembled on graphene as enhanced catalyst for oxygen reduction reaction. *J. Am. Chem. Soc.* **2012**, *134*, 2492–2495.

[62] Groves, M. N.; Malardier-Jugroot, C.; Jugroot, M. Improving platinum catalyst durability with a doped graphene support. *J. Phys. Chem. C* **2012**, *116*, 10548–10556.

[63] Choi, C. H.; Park, S. H.; Woo, S. I. Binary and ternary doping of nitrogen, boron, and phosphorus into carbon for enhancing electrochemical oxygen reduction activity. *ACS Nano* **2012**, *6*, 7084–7091.

[64] Liang, J.; Jiao, Y.; Jaroniec, M.; Qiao, S. Z. Sulfur and nitrogen dual-doped mesoporous graphene electrocatalyst for oxygen reduction with synergistically enhanced performance. *Angew. Chem. Int. Edit.* **2012**, *51*, 11496–11500.

[65] Wang, H.; Maiyalagan, T.; Wang, X. Review on recent progress in nitrogen-doped graphene: Synthesis, characterization, and its potential applications. *ACS Catal.* **2012**, *2*, 781–794.

[66] Ding, W.; Wei, Z.; Chen, S.; Qi, X.; Yang, T.; Hu, J.; Wang, D.; Wan, L. J.; Alvi, S. F.; Li, L. Space-confinement-induced synthesis of pyridinic- and pyrrolic-nitrogen-doped graphene for the catalysis of oxygen reduction. *Angew. Chem. Int. Edit.* **2013**, *52*, 11755–11759.

[67] Liu, S. H.; Wu, M. T.; Lai, Y. H.; Chiang, C. C.; Yu, N.; Liu, S. B. Fabrication and electrocatalytic performance of highly

stable and active platinum nanoparticles supported on nitrogen-doped ordered mesoporous carbons for oxygen reduction reaction. *J. Mater. Chem.* **2011**, *21*, 12489–12496.

[68] Wu, G.; Li, D.; Dai, C.; Wang, D.; Li, N. Well-dispersed high-loading Pt nanoparticles supported by shell–core nanostructured carbon for methanol electrooxidation. *Langmuir* **2008**, *24*, 3566–3575.

[69] He, D.; Jiang, Y.; Lv, H.; Pan, M.; Mu, S. Nitrogen-doped reduced graphene oxide supports for noble metal catalysts with greatly enhanced activity and stability. *Appl. Catal. B: Environ.* **2013**, 379–388.

[70] Muhich, C. L.; Westcott, J. Y.; Morris, T. C.; Weimer, A. W.; Musgrave, C. B. The effect of N and B doping on graphene and the adsorption and migration behavior of Pt atoms. *J. Phys. Chem. C* **2013**, *117*, 10523–10535.

[71] Vinayan, B. P.; Nagar, R.; Rajalakshmi, N.; Ramaprabhu, S. Novel platinum–cobalt alloy nanoparticles dispersed on nitrogen-doped graphene as a cathode electrocatalyst for PEMFC applications. *Adv. Funct. Mater.* **2012**, *22*, 3519–3526.

[72] Li, Y. H.; Hung, T. H.; Chen, C. W. A first-principles study of nitrogen- and boron-assisted platinum adsorption on carbon nanotubes. *Carbon* **2009**, *47*, 850–855.

[73] Yang, Z.; Yao, Z.; Li, G.; Fang, G.; Nie, H.; Liu, Z.; Zhou, X.; Chen, X. A.; Huang, S. Sulfur-doped graphene as an efficient metal-free cathode catalyst for oxygen reduction. *ACS Nano* **2011**, *6*, 205–211.

[74] Higgins, D.; Hoque, M. A.; Seo, M. H.; Wang, R.; Hassan, F.; Choi, J. Y.; Pritzker, M.; Yu, A.; Zhang, J.; Chen, Z. Development and simulation of sulfur-doped graphene supported platinum with exemplary stability and activity towards oxygen reduction. *Adv. Funct. Mater.* **2014**, *24*, 4325–4336.

[75] Galeano, C.; Meier, J. C.; Peinecke, V.; Bongard, H.; Katsounaros, I.; Topalov, A. A.; Lu, A.; Mayrhofer, K. J. J.; Schüth, F. Toward highly stable electrocatalysts via nanoparticle pore confinement. *J. Am. Chem. Soc.* **2012**, *134*, 20457–20465.

[76] Wang, X. X.; Tan, Z. H.; Zeng, M.; Wang, J. N. Carbon nanocages: A new support material for Pt catalyst with remarkably high durability. *Sci. Rep.* **2014**, *4*, 4437.

[77] Zhang, C. W.; Xu, L. B.; Shan, N. N.; Sun, T. T.; Chen, J. F.; Yan, Y. S. Enhanced electrocatalytic activity and durability of Pt particles supported on ordered mesoporous carbon spheres. *ACS Catal.* **2014**, *4*, 1926–1930.

[78] Santiago, D.; Rodríguez-Calero, G. G.; Palkar, A.; Barraza-Jimenez, D.; Galvan, D. H.; Casillas, G.; Mayoral, A.; Jose-Yacamán, M.; Echegoyen, L.; Cabrera, C. R. Platinum electrodeposition on unsupported carbon nano-onions. *Langmuir* **2012**, *28*, 17202–17210.

[79] Ho, V. T. T.; Pan, C. J.; Rick, J.; Su, W. N.; Hwang, B. J. Nanostructured $Ti_{0.7}Mo_{0.3}O_2$ support enhances electron transfer to Pt: High-performance catalyst for oxygen reduction reaction. *J. Am. Chem. Soc.* **2011**, *133*, 11716–11724.

[80] Kumar, A.; Ramani, V. Strong metal–support interactions enhance the activity and durability of platinum supported on tantalum-modified titanium dioxide electrocatalysts. *ACS Catal.* **2014**, *4*, 1516–1525.

[81] Xia, M.; Ding, W.; Xiong, K.; Li, L.; Qi, X.; Chen, S.; Hu, B.; Wei, Z. Anchoring effect of exfoliated-montmorillonite-supported Pd catalyst for the oxygen reduction reaction. *J. Phys. Chem. C* **2013**, *117*, 10581–10588.

[82] Ding, W.; Xia, M. R.; Wei, Z. D.; Chen, S. G.; Hu, J. S.; Wan, L. J.; Qi, X. Q.; Hu, X. H.; Li, L. Enhanced stability and activity with Pd–O junction formation and electronic structure modification of palladium nanoparticles supported on exfoliated montmorillonite for the oxygen reduction reaction. *Chem. Commun.* **2014**, *50*, 6660–6663.

[83] Yang, M.; Cui, Z.; DiSalvo, F. J. Mesoporous titanium nitride supported Pt nanoparticles as high performance catalysts for methanol electrooxidation. *Phys. Chem. Chem. Phys.* **2013**, *15*, 1088–1092.

[84] Roca-Ayats, M.; García, G.; Galante, J. L.; Peña, M. A.; Martínez-Huerta, M. V. Electrocatalytic stability of Ti based-supported Pt_3Ir nanoparticles for unitized regenerative fuel cells. *Int. J. Hydrogen Energy* **2014**, *39*, 5477–5484.

[85] Qiu, Z.; Huang, H.; Du, J.; Tao, X.; Xia, Y.; Feng, T.; Gan, Y.; Zhang, W. Biotemplated synthesis of bark-structured TiC nanowires as Pt catalyst supports with enhanced electrocatalytic activity and durability for methanol oxidation. *J. Mater. Chem. A* **2014**, *2*, 8003–8008.

[86] Kimmel, Y. C.; Xu, X.; Yu, W.; Yang, X.; Chen, J. G. Trends in electrochemical stability of transition metal carbides and their potential use as supports for low-cost electrocatalysts. *ACS Catal.* **2014**, *4*, 1558–1562.

[87] Avasarala, B.; Haldar, P. Durability and degradation mechanism of titanium nitride based electrocatalysts for PEM (proton exchange membrane) fuel cell applications. *Energy* **2013**, *57*, 545–553.

[88] Zhang, R. Q.; Lee, T. H.; Yu, B. D.; Stampfl, C.; Soon, A. The role of titanium nitride supports for single-atom platinum-based catalysts in fuel cell technology. *Phys. Chem. Chem. Phys.* **2012**, *14*, 16552–16557.

[89] Ma, X.; Meng, H.; Cai, M.; Shen, P. K. Bimetallic carbide nanocomposite enhanced Pt catalyst with high activity and stability for the oxygen reduction reaction. *J. Am. Chem. Soc.* **2012**, *134*, 1954–1957.

[90] Xie, X.; Chen, S.; Ding, W.; Nie, Y.; Wei, Z. An extraordinarily stable catalyst: Pt NPs supported on two-dimensional

$Ti_3C_2X_2$ (X = OH, F) nanosheets for oxygen reduction reaction. *Chem. Commun.* **2013**, *49*, 10112– 10114.

[91] Xie, X.; Xue, Y.; Li, L.; Chen, S.; Nie, Y.; Ding, W.; Wei, Z. Surface Al leached Ti_3AlC_2 substituting carbon for catalyst support served in a harsh corrosive electrochemical system. *Nanoscale* **2014**, *6*, 11035–11040.

[92] Lv, H.; Mu, S. Nano-ceramic support materials for low temperature fuel cell catalysts. *Nanoscale* **2014**, *6*, 5063–5074.

[93] Li, Y.; Li, Y.; Zhu, E.; McLouth, T.; Chiu, C. Y.; Huang, X.; Huang, Y. Stabilization of high-performance oxygen reduction reaction Pt electrocatalyst supported on reduced graphene oxide/carbon black composite. *J. Am. Chem. Soc.* **2012**, *134*, 12326–12329.

[94] Ramesh, P.; Itkis, M. E.; Tang, J. M.; Haddon, R. C. SWNT−MWNT hybrid architecture for proton exchange membrane fuel cell cathodes. *J. Phys. Chem. C* **2008**, *112*, 9089–9094.

[95] Wang, Y. J.; Wilkinson, D. P.; Neburchilov, V.; Song, C.; Guest, A.; Zhang, J. Ta and Nb co-doped TiO_2 and its carbon-hybrid materials for supporting Pt–Pd alloy electrocatalysts for PEM fuel cell oxygen reduction reaction. *J. Mater. Chem. A* **2014**, *2*, 12681–12685.

[96] Kou, R.; Shao, Y.; Mei, D.; Nie, Z.; Wang, D.; Wang, C.; Viswanathan, V. V.; Park, S.; Aksay, I. A.; Lin, Y.; et al. Stabilization of electrocatalytic metal nanoparticles at metal−metal oxide−graphene triple junction points. *J. Am. Chem. Soc.* **2011**, *133*, 2541–2547.